Maternal Ezh1/2 deficiency in oocyte delays H3K27me2/3 restoration and impairs epiblast development responsible for embryonic sub-lethality in mouse

Yinan Zhao[1#], Dandan Bai[2#], You Wu[2#], Dan Zhang[1], Mengying Liu[1], Yingpu Tian[1], Jinhua Lu[3], Haibin Wang[3*], Shaorong Gao[2*], Zhongxian Lu[1,3*]

[1] School of Pharmaceutical Sciences, State Key Laboratory of Cellular Stress Biology, Xiamen University, Xiamen, Fujian 361005, China

[2] Shanghai Key Laboratory of Signaling and Disease Research, School of Life Sciences and Technology, Tongji University, Shanghai 200092, China

[3] Fujian Provincial Key Laboratory of Reproductive Health Research, Medical College of Xiamen University, Xiamen, Fujian 361102, China

***Correspondence:** Zhongxian Lu (zhongxian@xmu.edu.cn); Shaorong Gao，gaoshaorong@tongji.edu.cn； Haibin Wang, haibin.wang@vip.163.com

# These authors contributed equally

Key words: Ezh1, Ezh2, H3K27me3, embryonic development

Summary

Using maternal knockout mice models, Zhao et al. found that H3K27me2/3 restoration is delayed in preimplantation embryos and that the epiblast is compromised during development, revealing the role of PRC2-H3K27me3 in safeguarding pluripotent epiblast fate.

Abstract

How maternal Ezh1 and Ezh2 function in H3K27 methylation *in vivo* in preimplantation embryos and during embryonic development is not clear. Here, we deleted Ezh1 and Ezh2 alone or simultaneously from mouse oocytes. H3K27me3 was absent in oocytes without Ezh2 alone, while both H3K27me2 and H3K27me3 were absent in Ezh1/2 double knockout oocytes. The effects of Ezh1/2 maternal knockout were inherited in zygotes and early embryos, in which restoration of H3K27me3 and H3K27me2 was delayed by the loss of Ezh2 alone or of both Ezh1 and Ezh2. However, the ablation of both Ezh1 and Ezh2, but not Ezh1 or Ezh2 alone, led to significantly decreased litter size due to growth retardation during post-implantation. Maternal Ezh1/2 deficiency caused compromised H3K27me3 and pluripotent epiblast cells in late blastocysts, followed by defective embryonic development. By using RNA-seq, we examined critical developmental genes in maternal Ezh1/2 KO embryos and identified 80 putatively imprinted genes. Maternal Ezh1/2-H3K27 methylation is inherited in offspring embryos and has a critical effect on fetal and placental development. Thus, this work sheds light on maternal epigenetic modifications during embryonic development.

Introduction

Mammalian embryonic development begins with the formation of a zygote and ends when a fully developed fetus is delivered. This complex process is accompanied by a variety of epigenetic modifications (Saitou et al., 2012). Histone modifications are found to play key roles in epigenetic regulation (Canovas and Ross, 2016). Methylations at lysine 4, 9, and 27 on histone H3 act as transcriptional modulators and regulate specific sets of genes involved in embryogenesis, embryonic stem cell (ESC) pluripotency and differentiation, tissue stem cell maintenance, the establishment and maintenance of genomic imprinting, and tumorigenesis (Jambhekar et al., 2019; Michalak et al., 2019; Yu et al., 2019). Recently, dynamic patterns of H3K4 trimethylation (H3K4me3) and H3K27 trimethylation (H3K27me3), which play critical roles in maternal X-chromosome inactivation (XCI), zygotic genome

activation (ZGA) and developmental genes, have been illustrated in mouse oocytes and preimplantation embryos (Inoue et al., 2018; Liu et al., 2016; Zhang et al., 2016). Histone modifications are germline modifications that are inherited or reestablished during early embryogenesis (Liu et al., 2016; Zhang et al., 2016; Zheng et al., 2016). However, the regulation and underlying mechanisms of maternal histone modifications in embryonic development need to be fully explored.

PRC2 is a histone methyltransferase (HMT) complex that produces cell type-specific H3K27 mono- (H3K27me1), di- (H3K27me2), and trimethylation (H3K27me3) patterns (Bracken et al., 2006; Ferrari et al., 2014). H3K27me3 is a well-known repressive histone modification that ultimately causes transcriptional silencing (Cao et al., 2002). In mammals, the core subunits of the PRC2 complex include enhancer of zeste homolog 1 or 2 (Ezh1 or Ezh2), embryonic ectoderm development (Eed), suppressor of zeste 12 (Suz12) and retinoblastoma binding protein 4/7 (Rbbp4/7) (Yan et al., 2019). Ezh1 and Ezh2 are the catalytic subunits of the PRC2 complex (Margueron and Reinberg, 2011). In *Drosophila*, deletion of Enhancer of zeste [E(z)] during oogenesis causes embryonic lethality, even though H3K27me3 is reestablished in late zygotes (Zenk et al., 2017), indicating that H3K27me3 establishment during early embryogenesis requires maternal PRC2. However, the effects of maternal PRC2 on mammalian embryonic development remain unclear, and related reports are inconsistent. In mice, the oocyte-specific deletion of *Ezh2* by *Zp3-Cre* does not alter litter size but cause growth retardation in the progeny (Erhardt, 2003). Maternal *Eed* knockout by *Gdf9-Cre* shows loss of H3K27me3 imprinting and growth arrest in postimplantation (Inoue et al., 2018). Elimination of *Eed* from growing oocytes by *Zp3-Cre* results in a significant overgrowth phenotype that persists into adult life (Prokopuk et al., 2018). These results indicate that *Ezh2* and *Eed* may have different functions in postembryonic development (Prokopuk et al., 2018). Collectively, these discoveries suggest that maternal PRC2 core components have a long-term effect on the development of mother's descendant. However, the exact details of this process remain to be discovered. Recently, a report showed that Ezh2 is required for the establishment of

H3K27me3 in mouse zygotes, and Ezh1 could partially safeguard the role of Ezh2 (Meng et al., 2020), indicating that *Ezh1* might compensate for *Ezh2* in specific developmental contexts (Ezhkova et al., 2011; Mochizuki-Kashio et al., 2015). However, how maternal Ezh1 and Ezh2 comprehensively mediate H3K27 methylation in preimplantation embryos *in vivo* is unknown.

To investigate this issue, we used maternal *Ezh1/2* knockout mice to gain insights into the dynamic patterns of H3K27 methylation during the preimplantation period and reveal their regulatory effects on the embryonic development. The results demonstrated that maternal *Ezh1/2* are required for the establishment of H3K27me2/3 in preimplantation embryos *in vivo* and play critical roles in embryonic development in mouse.

Results

Recovery of H3K27me3 and H3K27me2 is delayed in early maternal knockout embryos

To reveal the maternal PRC2-mediated histone modifications and their long-term effects on embryonic development, we used an Ezh1 null mouse line and Gdf9-Cre transgenic mice to construct transgenic mouse models with *Ezh1* and *Ezh2* deletion in growing oocytes. Here, we established two pairs of mouse lines: sCtrl (single control, no *Ezh1* and *Ezh2* KO) and sKO (single knockout of Ezh2 in oocytes via Gdf9-Cre) **(sFig. 1A)**, and the other were dCtrl (double control, that is, *Ezh1* knockout) and dKO (double knockout of both *Ezh1* and *Ezh2* in oocytes) **(sFig. 2A)**. In sKO mice, the mRNA and protein levels of Ezh2 in the oocytes were undetectable **(sFig. 1B and 1C)**, whereas the expression of the other PRC2 core components, Ezh1, Eed, and Suz12, was not affected **(sFig. 1B)**. In dKO mice, the *Ezh1* and *Ezh2* genes were deleted, while the mRNA levels of *Eed* and *Suz12* were not affected **(sFig. 2B and 2C)**. These observations showed that Ezh1 and Ezh2 in oocytes were successfully deleted in oocytes in these mice.

The PRC2 complex is responsible for methylation of H3K27 through its enzymatic subunits Ezh1 and Ezh2 (Schuettengruber and Cavalli, 2009; Simon and Kingston, 2009). Then, we checked the H3K27me2/3 modifications in oocytes by immunohistochemistry (IHC) and immunofluorescence (IF). H3K27me3 was absent in oocytes from secondary follicles and MII oocytes from both sKO **(sFig. 1D and 1E)** and dKO mice **(sFig. 2D-2F)**. However, H3K27me2 was disappeared only in the MII oocytes of dKO mice, but not in those of sKO nor dCtrl mice **(sFig. 2F)**. These results suggest that Ezh2 is indispensable for H3K27me3 modification, while Ezh1 and Ezh2 can both facilitate H3K27me2 modification in oocytes.

Then, we examined the H3K27 methylation patterns at different stages of early embryos. Embryos from sCtrl, sKO, dCtrl and dKO females mated with wild-type males are hereafter referred to as sF (no Ezh1 and Ezh2 KO) /+, sKO(single EZH2 KO)/+, dF(single EZH1 KO)/+ and dKO (Ezh1 and Ezh2 KO)/+(with F representing flox), respectively. H3K27me3 staining was strong in the female pronucleus (PN) but relatively weak in the paternal PN in sF/+ late zygotes **(Fig. 1A)**. H3K27me3 was clearly detected in sF/+ embryos from the late 2-cell stage to the early blastocyst stage, while H3K27me3 staining was not restored until the late blastocyst stage in the sKO/+ groups **(Fig. 1A and sFig. 3A)**, suggesting that the modification of H3K27me3 in preimplantation embryos is dependent on maternal Ezh2. Enhanced H3K27me3 staining in the inner cell mass (ICM) appeared at the sKO/+ late blastocyst stage, along with dot staining in the trophectoderm (TE) in some embryos, which was comparable to that in sF/+ embryos **(Fig. 1A)**. In addition, H3K27me3 staining was still faint in late blastocysts of dKO/+ embryos **(Fig. 1B**, right images and **sFig. 3B)**, indicating that maternal Ezh1/2 have a long-lasting effect on H3K27me3 modification in early embryos.

During normal embryonic development, H3K27me2 and H3K27me3 have similar expression patterns. In sKO/+ embryos, the H3K27me2 in female PN was very weak in contrast to that in sF/+, and that in the paternal PN was almost undetectable **(Fig. 2A**, right images**)**. Furthermore, H3K27me2 in sKO/+ embryos was detected at the 2-cell stage and was comparable to that in sF/+ embryos at the 4-cell and morula

stages, followed by decreased intensity at the 8-cell and blastocyst stages **(Fig. 2A and sFig. 3C)**. However, H3K27me2 staining in dKO/+ embryos was absent from the zygotes to the 8-cell stage, faint from the morulae to the early blastocysts, and then fully recovered at the late blastocyst stage **(Fig. 2B**, right images and **sFig. 3D)**, indicating that maternal Ezh1 in conjunction with Ezh2 plays an important role in H3K27me2 modification.

Together, these observations demonstrate that H3K27 methylation activated by maternal PRC2 is dominant in preimplantation embryos and that maternal Ezh2 is required for H3K27me3 modification while maternal Ezh1 assists in H3K27me2 modification.

Double knockout of *Ezh1* and *Ezh2* in oocytes results in female subfertility

Next, we investigated the reproductive performance of the KO mice. KO females were mated with wild-type (WT) males. The cumulative number of pups, number of pups per litter and the number of litters per mouse were analyzed. The results showed that sKO females had normal fertility **(Fig. 3A-3C)**. While the cumulative number of pups produced from dKO females was obviously lower than that of dCtrl females **(Fig. 3D)**, the average litter size of dKO females (2.69 ± 1.35) was significantly smaller than that of dCtrl females (7.10 ± 2.13) **(Fig. 3E)**. The number of litters per mouse was also greatly decreased in dKO females **(Fig. 3F)**. These data suggest that the loss of both Ezh1 and Ezh2 in oocytes impaired female fertility in mice.

Maternal Ezh1/2 knockout embryos develop abnormally after implantation

Since histone modifications are broadly reprogrammed during gametogenesis (Matsui and Mochizuki, 2014; Zheng et al., 2016), we first examined ovary development and ovulation to reveal the cause of the subfertility. In dKO females, ovarian morphology was not affected and follicles developed normally **(sFig. 4A)**. The average number of ovulated oocytes in the dKO groups was also similar to that of dCtrl mice **(sFig. 4B and 4C)**. Moreover, there was no difference in the number of implantation sites on Day 5 of pregnancy between dKO and dCtrl females **(sFig. 4D**

and 4E), indicating that preimplantation development and embryo implantation were normal. These results suggest that the observed decrease in fertility is not due to defects in oogenesis and implantation.

Then, we focused on postimplantation embryos and isolated embryos at E10.5, when the mouse embryo is undergoing organogenesis (Kojima et al., 2014) and the basic structure of the mouse placenta is formed (Rossant and Cross, 2001). Morphologically, the development of the dKO/+ fetus and placenta appeared severely retarded at E10.5 **(Fig. 4A)**. Some embryos (26.83%) had been absorbed and could not be isolate **(Fig. 4B)**. In addition, the decidua weight of dKO females was greatly reduced compared to that of dCtrl females **(Fig. 4C)**, indicating growth restriction. HE staining showed that the phenotypes of the dKO/+ embryos at E10.5 could be identified into three categories. Type I had a placenta containing a labyrinth (Lab) layer, spongiotrophoblast (Sp) layer (always smaller) and trophoblast giant cells (TGC) **(Fig. 4D**, left second images**)**; type II had a fetus but had no Lab or Sp **(Fig. 4D**, right second images**)**; and type III embryos were partially or completely absorbed **(Fig. 4D**, right first images**)**.

Furthermore, growth retardation of embryos from E5.5-E7.5 was observed in decidual sections **(Fig. 4E**, E5.5-E7.5**)**. Indeed, analysis of paraffin sections and tissue dissection under stereoscope showed that the embryos decreased in size beginning at E5.5. Moreover, failure of chorioallantoic attachment and branching was observed in dKO/+ embryos at E9.5, in line with the placental defects observed at E10.5 **(Fig. 4E)**. This demonstrates that growth arrest during postimplantation phase is responsible for the subfertility in these mice. It is known that chorioallantoic attachment during placental development is dependent on Vcam1, a cell-adhesion molecule that is expressed on the tip of the allantois, and its ligand integrin α4, which is expressed on the basal surface of the chorion (Rossant and Cross, 2001). However, IHC analysis showed that Vcam1 and integrin α4 were expressed normally in dKO/+ embryos **(Fig. 4F and 4G)**, indicating that the interactions between Vcam1 and integrin α4 alone are not sufficient for a successful union of the chorion and allantois (Walentin et al., 2016)

and other factors may account for the failed chorioallantoic attachment observed in dKO/+ embryos.

Surprisingly, morphological and histological analyses revealed that the placentas of dKO/+ embryos were enlarged in the late stage of pregnancy **(Fig. 5A and 5B)**, as indicated by the overgrowth of spongiotrophoblasts and increased placental weight at E17.5 **(Fig. 5C and 5F)**. However, the fetuses were smaller than those in the dF/+ groups **(Fig. 5A)**, with decreased weight and length **(Fig. 5D and 5E)**.

In summary, the development defects of the embryos fell into three distinct categories. Embryos in the first category ceased development shortly after implantation and could not develop past gastrulation; those in the second category failed to establish placentation and were destined to death; and those in the third category successfully achieved gastrulation and placentation but were accompanied by giant placenta and fetal growth restriction.

To determine whether the maternal uterine environment contributed to the observed growth retardation, embryo transfer experiments were pursued. dF/+ and dKO/+ blastocysts were separately transferred to WT pseudopregnant recipients. The dKO/+ groups showed a considerably reduced number of term pups (**Supplementary Table 1**). This result was consistent with the subfertility of dKO females. Approximately 18% of the dKO/+ blastocysts developed to term pups, much lower than the rate for dF/+ blastocysts (about 48%) (**Supplementary Table 1**). This finding indicates that defects in the dKO/+ embryo *per se*, rather than the maternal uterine environment, contributes to abnormal embryonic development.

Above all, these results suggest that maternal Ezh1/2 deficiency in oocytes disturbs the embryonic development and that the loss of maternal Ezh1/2 has a long-lasting consequence for embryogenesis.

EPI cells are abnormal in dKO/+ embryos during peri-implantation

To trace the onset and progression of developmental abnormalities, the development of dKO/+ embryos was examined during peri-implantation in mice. Normally, epiblast (EPI) cells differentiated from the inner cell mass (ICM)

proliferate rapidly after implantation, and then the embryos form a proamniotic cavity at E5.5, a prerequisite for gastrulation (Mole et al., 2020; Tam and Loebel, 2007). However, no discernible epiblast was observed in dKO/+ embryos at E4.75 **(Fig. 6A)**. Successive sections showed that dKO/+ embryos had few Oct4+ cells at E4.75 **(Fig. 6B and sFig.7A)**. At E5.5, dKO/+ embryos had no proamniotic cavity with reduced EPI area while dF/+ embryos showed an obvious proamniotic cavity **(Fig. 6C and sFig.7B)**. Our careful morphological examinations at different embryonic stages reveal that growth arrest occurs during peri-implantation period and that EPI/ICM development is defective.

We next sought to determine how the EPI/ICM cells are impaired. In mouse development, the first cell lineage decision occurs prior to implantation (around at E3.0~3.5) and generates two cell populations: TE cells expressing the *Cdx2* genes and ICM cells expressing the *Oct4* gene (Chazaud and Yamanaka, 2016). We examined the first cell fate decision by immunostaining with Oct4 and Cdx2 at E3.75. There was no difference in TE and ICM cell allocation between dF/+ and dKO/+ embryos **(Fig. S5A)**. Neither the number of ICM and TE cells nor their ratios were significantly changed, although the number of cells expressing both factors was increased in dKO/+ embryos **(Fig. S5B and 5C)**. Thus, the first cell fate decision appears to be normal in embryos with maternal *Ezh1/2* deletion.

The second cell lineage decision, occurring during implantation, segregates the ICM into EPI cells and primitive endoderm (PrE) cells that express Nanog and Gata6, respectively (Chazaud and Yamanaka, 2016). EPI cells produce the fetus, while the PrE cells and trophectoderm produce extraembryonic tissues (DePamphilis, 2016). The phenotypic similarity between dKO/+ embryos and *Nanog* null mice at the peri-implantation period (Mitsui et al., 2003) prompted us to examine whether the loss of maternal *Ezh1/2* results in the dysregulation of the second cell fate decision. As shown in Fig. 7, the morphology of E4.5 dKO/+ embryos was not different from that of dF/+ embryos at the same stage **(Fig. 7A)**. While the expression of Nanog and Gata6 was observed in late blastocysts **(Fig. 7B)**, Nanog-positive (Nanog+) cells in dKO/+ embryos were obviously fewer in number than that in dF/+ embryos,

indicating that EPI cells were reduced **(Fig. 7B)**. Cell counts showed that the cell numbers of dF/+ and dKO/+ embryos were nearly equivalent **(Fig. 7C)**, while EPI cells in dKO/+ embryos were remarkably reduced (6.83 ± 3.24) compared to those in dF/+ embryos (11.58 ± 3.00) **(Fig. 7C)**. Unexpectedly, the PrE cell number was significantly decreased, to around 66% of that of dF/+ embryos **(Fig. 7C)**. Moreover, the ratios of both EPI and PrE were obviously reduced **(Fig. 7D)**. The TE cell number was not significantly changed, but its ratio to the total cell number was obviously increased, while mixed-expressed cells appeared and accounted for about 4.21% of total cells **(Fig. 7C and 7D)**. Consistent with this result, Oct4 and Gata6 were expressed in late blastocysts **(sFig. 6A)**. The average cell numbers per embryo was not changed significantly **(sFig. 6B)**, but the number of Oct4+ only cells was obviously decreased in dKO/+ embryos at E4.5 **(sFig. 6C and 6D)**. These results show that maternal *Ezh1/2* deletion impaired the second cell fate decision, leading to fewer EPI cells and more cells with mixed stem cell markers expression during implantation.

It has been shown that the promoters of developmental genes are strongly marked with H3K27me3 in EPI in postimplantation embryos (Rugg-Gunn et al., 2010; Zheng et al., 2016).Therefore, we hypothesized that the defects in second lineage commitment may be associated with reduced H3K27me3 signals. To test this hypothesis, we examined H3K27me3 modification and Nanog expression in embryos at E4.5. In addition to punctate H3K27me3 signals in some embryos, H3K27me3 modification appeared in Nanog+ cells and was apparently reduced in dKO/+ embryos and almost absent in Gata6+ cells of both dF/+ and dKO/+ late blastocysts **(Fig. 7E and sFig. 7C)**. We found strong correlations between Nanog+ cells and H3K27me3 modification in both dF/+ and dKO/+ embryos **(sFig. 7D)**. However, the number of Nanog+ and H3K27me3+ cells was not notably different between sF/+ and sKO/+ late blastocysts, although they exhibited an obvious correlation in both sF/+ and sKO/+ embryos **(sFig.8)**. These observations suggested that EPI development is associated with H3K27me3 modification.

In summary, the maternal Ezh1/2 is crucial for second cell lineage determination and propagation of the EPI state during implantation.

Identifying differentially expressed genes and putative imprinted genes in dKO/+ embryos

To further examine how maternal Ezh1/2 KO caused embryonic growth arrest, we performed RNA-seq at the morula stage and E7.5 **(Fig. 8A and 8B)**. Few DEGs were identified in morulae, while thousands of DEGs were found in both the EPI and ExE at E7.5 **(Fig. 8C)**. GO analysis showed that many DEGs were enriched in the stem cell population and over the course of embryonic development **(Fig. 8D)**. The expression of essential genes associated with stem cell identity and embryonic development, such as Fgf4 and Sox2 in EPI and Cdx2, Ascl2 and Slc34a2 in ExE, were remarkably decreased **(Fig. 8E)**. This result indicates that embryonic arrest is probably caused by stem cell defects.

Previous studies have demonstrated that Eed maternal KO causes embryonic lethality and loss of H3K27me3 imprinting (Inoue et al., 2018). To investigate whether maternal Ezh1/2 KO also causes a loss of H3K27me3 imprinting, we performed PN exchange and RNA-seq **(Fig. 8A and 8B)**. Although only a few DEGs were discovered in the morula, one of these genes, *Rlim* which is involved in random inactivation of X chromosome (Barakat et al., 2011; Shin et al., 2010), was decreased expressed (LogFC = -1.4065 and FDR = 0.042762) **(Fig. 8B)**. This reminded us to analyze the gene expression of X chromosome genes. Genes on the X chromosome were specifically down-regulated **(Fig. 8F)**. Thus, the X chromosome inactivation may be affected by maternal Ezh1/2 KO. To examine the allelic gene expression and screen putative H3K27m3-dependent imprinted genes, we performed RNA-seq on PN exchanged morulas **(Fig. 8A and 8B)**. Eighty genes, including Xist, Gramd1b and Epas1, were identified as putative H3K27me3-dependent imprinted genes **(Fig. 8G** and (Supplementary Table 4**)**. To examine the allelic H3K27me3 modification of these genes, ChIP-seq data from maternal Eed KO (Inoue et al., 2018) were used. Among the 80 genes, 26 showed maternal H3K27me3 modification at their promoters

(Supplementary Table 4). These results suggest that maternal Ezh1/2 KO caused a loss of H3K27me3-dependent imprinting.

Discussion

Our study investigated the effects of maternal *Ezh1/2* on H3K27 methylation patterns and mouse embryonic development by deleting *Ezh1* and *Ezh2* in oocytes. We reveal that *Ezh2* is required for H3K27me3 and that *Ezh1* partially complements *Ezh2* for H3K27me2 in oocytes. The effect of maternal *Ezh1/2* was inherited in descendant embryos. Loss of maternal *Ezh1/2* causes a delay in the restoration of H2K27me2/3 modification in preimplantation embryos *in vivo*. We also demonstrated that the loss of maternal *Ezh1/2* has long-term developmental consequences, resulting in growth retardation. Maternal *Ezh1/2* is essential for second lineage determination and EPI cell fate during implantation. Critical developmental genes were dysregulated in postimplantation embryos, and putative H3K27me3-dependent imprinted genes were identified. These findings uncover the essential function of maternal *Ezh1/2* on H3K27me2/3 modification and embryonic development, providing a novel understanding of embryonic development regulation by epigenetic modulators.

Maternal *Ezh1* and *Ezh2* in descendant development in mice

It has been shown that Ezh1 and Ezh2 are functionally redundant (Ezhkova et al., 2009; Margueron et al., 2008; Shen et al., 2008), and tissues deficient in *Ezh1* and *Ezh2* show more severe defects than those lacking only *Ezh2* (Ezhkova et al., 2011; Mochizuki-Kashio et al., 2015). This is also the case in our work. Previous reports indicated that mice lacking *Ezh1* were normal (Ezhkova et al., 2011), while oocyte-specific deletion of *Ezh2* induced growth retardation in offspring but did not influence mouse fertility (Erhardt, 2003), which is consistent with the fertility performance of dCtrl and sKO females in the present work. In our mouse model, double knockout of *Ezh1* and *Ezh2*, but not *Ezh1* or *Ezh2* alone, in oocytes caused embryonic sublethality, suggesting that *Ezh1* complements (or partially complements)

Ezh2 function in embryonic development and that maternal *Ezh2* and *Ezh1* work together governs the descendant development. Notably, the patterns of H3K27me3 in late blastocysts and the breeding results were consistent to some extent. Considering that H3K27me3 modification is associated with pluripotent EPI, it is possible that the pattern of H3K27me3 during the peri-implantation period may determine the embryonic development potential, which might explain the fertility discrepancy between different groups.

Maternal *Ezh1* and *Ezh2* in H3K27 methylation in preimplantation embryos *in vivo*

Our knockout mouse model showed that Ezh2 is required for H3K27me3 and that *Ezh1* complements *Ezh2* in H3K27me2 in oocytes. The effect of *Ezh1/2* is inherited in maternal knockout zygotes. H3K27me3 was lost in the sKO/+ and dKO/+ maternal PN while H3K27me2 was reduced in the sKO/+ female PN but absent in the dKO/+ female PN. The H3K27me2 signal was almost undetectable in both the paternal and maternal PN in the dKO/+ zygotes, similar to the H3K27me2 pattern in Eed m-/p+ zygotes, but different from a prior report in which the H3K27me2 of maternal PN was normal in Ezh2m-p+ *Ezh1* siRNA zygotes (Meng et al., 2020). In addition, the asymmetric parental H3K27me2/3 signal in the PNs of sF/+ and dF/+ zygotes is consistent with previous reports (Huang et al., 2014; Santos et al., 2005). Interestingly, similar patterns of H3K27me3 and H3K27me2 signals appeared in the paternal PN of maternal KO zygotes in this work. Normally, the histones in the paternal PN are initially hypomethylated and gradually acquire H3K27me2/3 modifications in late zygotes due to a preferential recruitment of the PRC2 complex to maternal PNs; these marks become apparent in the paternal PN at later stages (Burton and Torres-Padilla, 2010; Erhardt, 2003). The lost deposition of H3K27me2/3 in the paternal PN of KO/+ zygotes indicates that the PRC2 complex is inactive in late zygotes or at least absent in the paternal PN. According to these results in our study, we speculate that *Ezh1* and *Ezh2* are required for *de novo* H3K27me2 in oocytes, which could be restored and inherited in the maternal PN in zygotes.

Deficiency of Ezh1 does not affect H3K27me2/3 patterns, while the loss of maternal Ezh2 alone or in combination with Ezh1 leads to delayed restoration of H3K27me2/3 in preimplantation embryos *in vivo*, indicating that maternal Ezh2 has a long-term effect on H3K27me2/3 in early embryos. However, the loss of H3K27me3 induced by Ezh2 single maternal KO did not affect embryo development. Potential explanations for this observation are as follows: (1) H3K27me3 is still enriched in the locus of imprinted genes despite the loss of H3K27me3 staining; in this case, Ezh1 may safeguard this modification. H3K27me2/3 status in dKO/+ embryos is severely delayed compared with that in sKO/+, supporting this hypothesis and suggesting that Ezh1 compensating to sustain some residual PRC2 activity (Mochizuki-Kashio et al., 2015). (2) Imprinting os lost from some genes that are not critical to development. (3) extra epigenetic regulators probably guard the imprinting of critical genes in Ezh2 KO. These hypotheses are all need to be investigated.

However, the H3K27me2/3 patterns in *in vivo* preimplantation embryos in our study are different from those in previous reports (Erhardt, 2003; Inoue et al., 2018; Meng et al., 2020). H3K27me3 was not recovered in early blastocysts of sKO/+ and dKO/+ embryos in our research. Erhardt et al. showed that a normal H3K27me3 pattern emergence in maternal Ezh2 knockout embryos (16-cell stage), but after the time of embryonic Ezh2 activation (Erhardt, 2003), while H3K27me3 of maternal Eed knockout embryos becomes comparable at the morula stage (Inoue et al., 2018). This difference may be attributable to differences in the collections of embryos, as histone modification may be changed by *in vitro* operation and culture (Kohda, 2013); alternatively, activation of Ezh1/2 may occur later than activation of Eed in maternal knockout embryos. Additionally, the conversation to histone methylation to H3K27me3 is more time-consuming than conversion of H2K27me1 and H3K27me2 (Anne Laugesen et al., 2019), and recent work indicated that H3K27me2 might be a critical prerequisite for de novo H3K27me3 (Meng et al., 2020). Therefore, the delayed restoration of H3K27me3 may be induced by deferred H3K27me2. In dKO/+ preimplantation embryos, H3K27me2 appeared beginning at the morula stage and completely recovered at the late blastocyst stage. Since Ehmt1 is also involved in the

establishment of H3K27me2 (Meng et al., 2020), we suppose that this may be associated with delayed embryonic Ezh1/2 or Ehmt1 transcription to initiate H3K27me2. This hypothesis should be verified in the future work.

Above all, it can be stated that the capacity of H3K27 methylation reprogramming in preimplantation embryos was compromised by the deletion of maternal Ezh2 alone or in combination with Ezh1.

Maternal PRC2-H3K27me3 in the second cell fate decision and embryonic development

Erhardt et al. suggested that Ezh2 may be crucial for the propagation of the pluripotency and for cell fate determination during the early stages of embryonic development (Erhardt, 2003). In this work, we reveal that maternal loss of Ezh1/2 leads to a reduction in EPI cell number and defective second cell fate specification during implantation, revealing the importance of Ezh1/2 and H3K27me3 for the EPI state and cell fate decisions. Therefore, the fact that stem cells from Ezh2 mutant embryos are difficult to established and show impaired potential for outgrowth (O'Carroll et al., 2001) may be associated with pluripotency failure EPI cells due to a lack of Ezh2 and H3K27me3.

It is now clear that a reduction in ICM cell numbers diminishes embryogenetic potential (Tam, 1988). The initiation of gastrulation is suggested to require the attainment of some threshold, either a minimum cell number or a certain tissue mass of EPI (Kojima et al., 2014). Our results showed a markedly decrease in the number of ICM/EPI cells in dKO/+ embryos during implantation. Fgf4 and Sox2 are pluripotency markers associated with both pre- and postimplantation EPI (Boroviak et al., 2015). Moreover, Oct4 and Sox2 collaboratively induce the expression of genes essential for maintaining pluripotency, including their own, Nanog and Fgf4 (Rizzino and Wuebben, 2016). Considering reduced number of Oct4+ and Nanog+ only cells during the peri-implantation phase and decreased expression of Fgf4 and Sox2 in postimplantation, it is suggested that the Sox2, Oct4, Nanog and Fgf4 feedback loop was disrupted, resulting in embryo loss and growth retardation during gastrulation. It

is worth mentioning that the *in vitro* culture (IVC) system is a powerful tool for visualizing the EPI development and its surrounding tissues through the implantation stages (Bedzhov and Zernicka-Goetz, 2014; Morris et al., 2012). By using this system, the dynamics of blastocyst transformation into the egg cylinder will be directly revealed.

In our study, EPI cells (Nanog+) possessed H3K27me3 signals at E4.5 in both dF/+ and dKO/+ embryos. Similar H3K27me3 patterns were observed in previous reports (Erhardt, 2003; Liu et al., 2019). In ESCs, a set of genes are bivalently modified with H3K4me3 and H3K27me3, and remain "poised" (Liu et al., 2016; Rugg-Gunn et al., 2010). The withdrawal of PRC2 core components and H3K27me3 methylation results in bivalent derepression of genes and abnormal differentiation (Azuara et al., 2006; Boyer et al., 2006; Jorgensen et al., 2006; Lee et al., 2006). Considering the H3K27me3 modifications of developmental genes in EPI cells (Rugg-Gunn et al., 2010; Zheng et al., 2016), the decreased in Nanog+ cells may result from the deficiency of H3K27me3 and the derepression of cell fate-specific factors, which lead to differentiation into other lineages or mixed expression. A recent report demonstrated that in mouse ESCs, Nanog blocks differentiation by maintaining the H3K27me3 modification at developmental regulators (Heurtier et al., 2019). However, whether this regulatory network functions *in vivo* remains to be addressed in detail. For the two rounds of cell fate specification, cells in the wrong position or with ectopic expression of the transcriptional profile will eventually be cleared out by apoptosis (Zhu and Zernicka-Goetz, 2020). Whether the decreased number of ICM (EPI and PrE) cells is associated with increased apoptosis needs further assessment.

In brief, the loss of maternal Ezh1/2 and delayed restoration of H3K27 methylation change the epigenetic plasticity of pluripotent cells.

Maternal Ezh1/2 and gene imprinting in placental development

In maternal Ezh1/2 double KO mice, the development defects of the fetuses and placentas fell into three distinct categories. The cause of phenotypic variation may be related to epigenetic modification of maternal PRC2 on fetal and placental

development (Kohda, 2013; Lee et al., 2006). The process involves multiple factors, including the imprinting of many genes and the development of multiple cell types (Jambhekar et al., 2019; Jorgensen et al., 2006; Mei et al., 2021). Therefore, the long-term effects of maternal Ezh1/2 KO may vary based on the context in each embryo. The placental failure in our study is likely caused by multiple factors. It is known that a lack of chorioallantoic attachment and branching results in placental failure and embryonic mortality (Rossant and Cross, 2001; Walentin et al., 2016). Hence, in our work, failure of placentation in mid-gastrulation is at least one of the reasons for embryonic loss. But, it's not clear how the loss of maternal Ezh1/2 leads to chorioallantoic attachment failure; this error might be a byproduct of additional mechanisms (Inoue et al., 2018; Perez-Garcia et al., 2018). Fgf4 is expressed by EPI during implantation development and is necessary for trophoblast stem cell proliferation (Boroviak et al., 2015; Christodoulou et al., 2019; Tanaka et al., 1998). Thus, the diminished Cdx2 in ExE at E7.5 and placental failure may be caused by lower Fgf4 in EPI, which is a secondary effect of maternal Ezh1/2 KO. Additionally, mash2 mutants die from placental failure at around E10, and in Slc34a2 mutants, the placental labyrinth is absent (Guillemot et al., 1997; Shibasaki et al., 2009).

H3K27me3-modified imprinted genes are found to play important roles in placental development(Inoue et al., 2020). Several imprinted genes, including Slc38a4, Sfmbt2 and Gab1, remain their imprinting state in the placenta (Inoue et al., 2018). Deletion of these gene in mouse causes the defect of placenta and fetus (Mei et al., 2021). Here, we have also obtained 80 putative H3K27me3-dependent imprinted genes in our Ezh1/2 maternal KO morulas. So far, there are no other report on the H3K27me3 imprinting genes in Ezh1/2 or Ezh2 maternal KO embryos. But the H3K27me3-dependent imprinted genes have been analyzed in maternal Eed KO mouse embryos, and 26 of H3K27me3-dependent imprinted genes in our study were maternally marked according to their ChIP-seq data (Inoue et al., 2018). Three of these genes (Xist, Gramd1b and Epas1) were also reported to be imprinted by Inoue et al.(Inoue et al., 2018), indicating that maternal Ezh1/2 KO could lead to loss of H3K27me3-dependent imprinting.

In contrast, placentas enlargement was observed during the later development of dKO/+ embryos, characterized by expansion of the spongiotrophoblast layer. This phenotype was also reported in mouse embryos generated by somatic cell nuclear transfer (SCNT) (Tanaka et al., 2001). Some recent reports have demonstrated that the loss of H3K27me3 imprinting during SCNT contributes to placentomegaly in SCNT embryos, and that a more normal placenta weight could be restored by regulating H3K27me3-imprinted genes (Inoue et al., 2020; Matoba et al., 2018; Wang et al., 2020; Xie et al., 2022). However, placental enlargement is suggested to be associated with PRC1 complex, which guides the maternal inheritance and deposition of H3K27me3 in embryos (Chen et al., 2021; Mei et al., 2021).

Materials and Methods

Animals

Unless otherwise stated, the mice used in this study were of mixed background (129/SvJ and C57BL/6). The *Ezh2 loxp* and *Ezh1-/-* mice were gifts from Professor Alexander Tarakhovsky (The Rockefeller University, New York, USA). The mice were housed at Xiamen University Laboratory Animal Center under a 12 h light-dark cycle. Food and water were available *ad libitum* and room temperature was 24℃ with controlled humidity. All animal work was undertaken in accordance with the Xiamen University Animal Ethics Committee (approval no. 2015014). Genotyping was performed from tail DNA. Primers for genotype are shown in **Supplementary Table 2**.

Fertility studies

Fertility studies were performed as previously described (Andreu-Vieyra et al., 2008). To evaluate reproductive performance, individually caged females (2 months old) were bred with adult wild type males (C57BL/6J) of known fertility. After delivery, the number of pups was recorded. On the seventh day, the pups were removed, and the females and males continued to cage together. The breeding

experiment lasted six months. The number of litters and the number of pups were recorded during fertility study period.

Mating, implantation, embryo collection and decidua dissection

For basic embryological analyses, adult dCtrl and dKO females were naturally mated with adult wild type males (C57/BL6J). The morning on which a plug was found was counted as embryonic Day 0.5 (E0.5) or Day 1 of pregnancy. Implantation sites on Day 5 (09:00 am) of pregnancy were visualized by an intravenous injection of Chicago blue dye solution. Blastocysts were flushed from the uterine horn with M2 medium at E3.75 and E4.5. Deciduae of pregnant females were dissected from E4.75-E10.5. The fetuses and placentas were collected and dissected carefully under a stereoscope at E10.5 and E17.5.

Histology, immunohistochemistry and immunofluorescence

Tissues were fixed in 4% paraformaldehyde (PFA), dehydrated in ethanol, embedded in paraffin wax, and sectioned (5 μm). For tissue morphology observation, sections were stained with the hematoxylin-eosin (HE). For immunohistochemistry, sections were treated with 3% H_2O_2 for 20 minutes after antigen retrieval, followed by blocking for 1 hour in 5% bovine serum albumin (BSA). Sections incubated in primary antibodies overnight at 4 ℃ were subsequently treated with PV-9001 kits (ZSBIO) before being exposed to diaminobenzidine (DAB). Finally, sections were counterstained with hematoxylin. For immunofluorescence, after antigen retrieval, sections were blocked in 5% bovine serum albumin or 5% donkey serum and then incubated in primary antibodies overnight at 4 ℃. Then, the sections were washed in wash buffer and incubated with the appropriate Alexa-Fluor-conjugated secondary antibodies at 37 ℃ for 1 h. After staining with DAPI (Vector Laboratories), the samples were analyzed using confocal microscopy (Zeiss LSM 780). The antibodies are listed in **Supplementary Table 3**.

Oocyte and early embryo collection

MII oocytes were collected from females (3-5 weeks old) that have been superovulated by injection with PMSG and hCG (San-Sheng Pharmaceutical Co. Ltd). Preimplantation embryos were collected from superovulated females mated with adult wild type males (C57BL/6). Each set of embryos at a particular stage was flushed from the reproductive tract at defined time periods after hCG administration: 20 h (MII oocyte), 27-28 h (late zygote), 48 h (late 2-cell), 54-56 h (4-cell), 68-70 h (8-cell), 80 h (morula), 90-96 h (early blastocyst) and 120 h (late blastocyst).

Whole-mount immunostaining

Oocytes and embryos were fixed in 4% PFA containing 0.1% BSA for 20 min at room temperature. After that, all fixed samples were washed with PBS containing 0.1% BSA and permeabilized in 0.1% Triton X-100 in PBS with 0.1% BSA at room temperature for 30 min, and blocked in 1% BSA or 5% donkey serum in PBS at room temperature for 1 h. Blocked oocytes and embryos were incubated with primary antibodies at 4 ℃ overnight. Secondary antibodies were incubated at 37 ℃ for 1 h. After washing, the oocytes and embryos were mounted on a glass slide in DAPI. Fluorescence was detected under a laser-scanning confocal microscope (Zeiss, LSM 780).

Antibody-labeling

A 4AF647R-Antibody conjugation Kit (4A Biotech) was used to label H3K27me3 antibody with 4AF647R dyes. According to the labeling protocol, H3K27me3 antibody solutions (CST, 9733) were concentrated by ultrafiltration and were resuspended in PBS to 0.5-1 mg/ml, as indicated by the labeling protocol. An appropriate amount of antibody to be labeled was transferred to a clean tube. A 1/10 volume of reaction buffer was added to the tube with antibody and then mixed well. The vial was incubated in the dark for 30 min at room temperature. Labeled antibody solution was diluted with storage buffer, and stored in single use aliquots at -20 °C.

When performing immunofluorescence, labeled H3K27me3 was used after standard immunofluorescence staining with primary and secondary antibodies.

Quantitative real time PCR (QPCR) analyses

Oocyte preparation was performed as reported (Kim et al., 2015). RNA from oocytes was isolated using the SuperPrep Cell Lysis & RT Kit for real-time PCR (TOYOBO, Osaka, Japan). PCR was performed on the Agilent AriaMx Real-Time PCR System. Primers are listed in **Supplementary Table 2**. The relative transcripts amount was calculated by the cycle threshold method as described by Agilent using the AtiaMx Real-Time PCR System Software and normalized to the endogenous reference (*β-actin*). The relative amount of target gene expression for each sample was calculated and plotted as the mean ± SD.

Western blot analyses

Western blotting was carried out as previously described (Kim et al., 2015). Equal numbers of oocytes were collected in PBS containing 0.1% BSA. Proteins were isolated by centrifuging the oocytes at 12,000×g for 15 minutes at 4 ℃. The protein samples were then mixed and treated with 2×SDS buffer containing protease inhibitor. The protein molecules were separated by gel electrophoresis and transferred onto PVDF membranes. The membranes were blocked in 5% milk in TBST and then incubated with primary antibodies, followed by washing and incubation with second antibodies after washing. The band was detected with a Bio-Rad imaging system.

Vasectomy

Vasectomy was operated as previous documented (Bermejo-Alvarez et al., 2014). Wild type male mice (CD1) with a proven mating performance were selected and anesthetized. The abdomen surface was cleaned and wiped with 70% ethanol and then opened, and the vas deferens was exposed by gripping the testicular adipose pad with forceps. The vas deferens was cut and cauterized at two points simultaneously by using flame dressing forceps. The testicle, epididymis and vas deferens were moved

back to the abdominal cavity, and the procedure was repeated for the other side. The muscle and skin were sutured. The vasectomized male was moved to the cage placed on a warm stage and observed until it recovered from anesthesia. Wound clips were removed 14 days after vasectomy. The infertility of the vasectomized male was tested by mating fertile females before using them to obtain recipients.

Embryo transfer

Embryo transfer was performed as previously described (Bermejo-Alvarez et al., 2014). Female mice were superovulated and mated with wild type males (C57BL/6). Blastocysts were flushed out of the uteri on Day 4 of pregnancy, then transferred into the uteri of pseudopregnant female mice (CD1, wild type) mated with vasectomized males. About 17 days after embryo transfer, the recipients were examined for the presence of a fetus. The number of fetuses was recorded.

RNA-seq library preparation and sequencing

Libraries for RNA-seq were constructed with Smart-seq2 (Picelli et al., 2014). Cells were washed at least three times with 0.5% BSA-PBS and picked into lysis buffer by mouth pipetting. After cell lysis and reverse transcription, the cDNA was amplified for 18 cycles in a thermal cycler. The products were fragmented with a Covaris S220 instrument, and the libraries were constructed with a Kapa Hyper Prep kit (KAPA KK8504). The libraries were sequenced on an Illumina HiSeq 2500 with 125 bp single end sequencing, and quality control was performed by the Berry Corporation. RNA-seq data processing was performed according to a previous report (Liu et al., 2016). ChIP-seq data (GSE116713) were downloaded from GEO(Inoue et al., 2018).

Analysis of H3K27me3 imprinting genes

We performed RNA-seq on PN-exchanged morulas and identified the putative H3K27m3-dependent imprinted genes according to the expression of genes in different PN exchanged morulas. An H3K27m3-dependent imprinted genes should be

that (1) its expression is low in wildtype female PN-exchanged morulas, but high in wildtype male PN-exchanged morulas; (2) the expression of this gene in wildtype female PN-exchanged morulas is clear lower than that in female Ezh1/2 KO (dKO) PN-exchanged morulas; (3) there was no difference in the expression of this gene in male PN-exchanged morulas between wild type and dKO.

Statistical analyses and data visualization

Statistical analyses were performed in GraphPad Prism 7. The quantitative data presented show the mean ± SD, percentages, or the total number of data points obtained. Levels of significance were calculated using the Mann-Whitney test, unpaired *t* test or χ^2 test. In all figures: ns, not significant; *, $P < 0.05$; **, $P < 0.01$; ***, $P < 0.001$; ****, $P < 0.0001$.

Competing of interest

The authors declare no conflicts of interest.

Funding

This work was supported by the National Key Research and Development Program of China (grant no. 2018YFC1003701 and 2017YFC1001402) and the National Natural Science Foundation of China (grant no. 31970797 and 31671564).

Data availability

All data generated or analyzed during this study are included in this published article and its supplementary information files

Author contributions

Z. Lu and H. Wang conceived the original ideas, designed the project, and wrote the manuscript with inputs from Y. Zhao and S. Gao. Y. Zhao performed the majority of the experiments with participation from D. Zhang, M. Liu, J. Lu and Y. Tian.

Dandan Bai collected the morula and performed pronucleus exchange for RNA-seq. Dandan Bai performed RNA-seq and You Wu analyzed the sequencing datasets. All authors read and approved the final manuscript.

Acknowledgments

We gratefully thank Professor Alexander Tarakhovsky at Rockefeller University (New York, USA) for the gift of transgenic mice.

Reference

Andreu-Vieyra, C., Chen, R., Matzuk, M.M., 2008. Conditional deletion of the retinoblastoma (Rb) gene in ovarian granulosa cells leads to premature ovarian failure. Mol Endocrinol 22, 2141-2161.

Anne Laugesen, Jonas Westergaard Højfeldt, Helin, a.K., 2019. Molecular Mechanisms Directing PRC2 Recruitment and H3K27 Methylation. Mol Cell 74, 8-18.

Azuara, V., Perry, P., Sauer, S., Spivakov, M., Jorgensen, H.F., John, R.M., Gouti, M., Casanova, M., Warnes, G., Merkenschlager, M., Fisher, A.G., 2006. Chromatin signatures of pluripotent cell lines. Nat Cell Biol 8, 532-538.

Barakat, T.S., Gunhanlar, N., Pardo, C.G., Achame, E.M., Ghazvini, M., Boers, R., Kenter, A., Rentmeester, E., Grootegoed, J.A., Gribnau, J., 2011. RNF12 activates Xist and is essential for X chromosome inactivation. PLoS Genet 7, e1002001.

Bedzhov, I., Zernicka-Goetz, M., 2014. Self-organizing properties of mouse pluripotent cells initiate morphogenesis upon implantation. Cell 156, 1032-1044.

Bermejo-Alvarez, P., Park, K.E., Telugu, B.P., 2014. Utero-tubal embryo transfer and vasectomy in the mouse model. J Vis Exp, e51214.

Boroviak, T., Loos, R., Lombard, P., Okahara, J., Behr, R., Sasaki, E., Nichols, J., Smith, A., Bertone, P., 2015. Lineage-Specific Profiling Delineates the Emergence and Progression of Naive Pluripotency in Mammalian Embryogenesis. Dev Cell 35, 366-382.

Boyer, L.A., Plath, K., Zeitlinger, J., Brambrink, T., Medeiros, L.A., Lee, T.I., Levine, S.S., Wernig, M., Tajonar, A., Ray, M.K., Bell, G.W., Otte, A.P., Vidal, M., Gifford, D.K., Young, R.A., Jaenisch, R., 2006. Polycomb complexes repress developmental regulators in murine embryonic stem cells. Nature 441, 349-353.

Bracken, A.P., Dietrich, N., Pasini, D., Hansen, K.H., Helin, K., 2006. Genome-wide mapping of Polycomb target genes unravels their roles in cell fate transitions. Genes Dev 20, 1123-1136.

Burton, A., Torres-Padilla, M.E., 2010. Epigenetic reprogramming and development: a unique heterochromatin organization in the preimplantation mouse embryo. Brief Funct Genomics 9, 444-454.

Canovas, S., Ross, P.J., 2016. Epigenetics in preimplantation mammalian development. Theriogenology 86, 69-79.

Cao, R., Wang, L., Wang, H., Xia, L., Erdjument-Bromage, H., Tempst, P., Jones, R.S., Zhang, Y., 2002. Role of histone H3 lysine 27 methylation in Polycomb-group silencing. Science 298, 1039-1043.

Chazaud, C., Yamanaka, Y., 2016. Lineage specification in the mouse preimplantation embryo. Development 143, 1063-1074.

Chen, Z., Djekidel, M.N., Zhang, Y., 2021. Distinct dynamics and functions of H2AK119ub1 and H3K27me3 in mouse preimplantation embryos. Nat Genet 53, 551-563.

Christodoulou, N., Weberling, A., Strathdee, D., Anderson, K.I., Timpson, P., Zernicka-Goetz, M., 2019. Morphogenesis of extra-embryonic tissues directs the remodelling of the mouse embryo at implantation. Nat Commun 10, 3557.

DePamphilis, M.L., 2016. Preface, Mammalian Preimplantation Development, pp. xiii-xxi.

Erhardt, S., 2003. Consequences of the depletion of zygotic and embryonic enhancer of zeste 2 during preimplantation mouse development. Development 130, 4235-4248.

Ezhkova, E., Lien, W.H., Stokes, N., Pasolli, H.A., Silva, J.M., Fuchs, E., 2011. EZH1 and EZH2 cogovern histone H3K27 trimethylation and are essential for hair follicle homeostasis and wound repair. Genes Dev 25, 485-498.

Ezhkova, E., Pasolli, H.A., Parker, J.S., Stokes, N., Su, I.H., Hannon, G., Tarakhovsky, A., Fuchs, E., 2009. Ezh2 orchestrates gene expression for the stepwise differentiation of tissue-specific stem cells. Cell 136, 1122-1135.

Ferrari, K.J., Scelfo, A., Jammula, S., Cuomo, A., Barozzi, I., Stutzer, A., Fischle, W., Bonaldi, T., Pasini, D., 2014. Polycomb-dependent H3K27me1 and H3K27me2 regulate active transcription and enhancer fidelity. Mol Cell 53, 49-62.

Guillemot, F., Nagy A Fau - Auerbach, A., Auerbach A Fau - Rossant, J., Rossant J Fau - Joyner, A.L., Joyner, A.L., 1997. Essential role of Mash-2 in extraembryonic development. Dev Biol 190, 55-65.

Heurtier, V., Owens, N., Gonzalez, I., Mueller, F., Proux, C., Mornico, D., Clerc, P., Dubois, A., Navarro, P., 2019. The molecular logic of Nanog-induced self-renewal in mouse embryonic stem cells. Nat Commun 10, 1109.

Huang, X.J., Wang, X., Ma, X., Sun, S.C., Zhou, X., Zhu, C., Liu, H., 2014. EZH2 is essential for development of mouse preimplantation embryos. Reproduction, fertility, and development 26, 1166-1175.

Inoue, A., Chen, Z., Yin, Q., Zhang, Y., 2018. Maternal Eed knockout causes loss of H3K27me3 imprinting and random X inactivation in the extraembryonic cells. Genes Dev 32, 1525-1536.

Inoue, K., Ogonuki, N., Kamimura, S., Inoue, H., Matoba, S., Hirose, M., Honda, A., Miura, K., Hada, M., Hasegawa, A., Watanabe, N., Dodo, Y., Mochida, K., Ogura, A., 2020. Loss of H3K27me3 imprinting in the Sfmbt2 miRNA cluster causes enlargement of cloned mouse placentas. Nat Commun 11, 2150.

Jambhekar, A., Dhall, A., Shi, Y., 2019. Roles and regulation of histone methylation in animal development. Nat Rev Mol Cell Biol 20, 625-641.

Jorgensen, H.F., Giadrossi, S., Casanova, M., Endoh, M., Koseki, H., Brockdorff, N., Fisher, A.G., 2006. Stem cells primed for action: polycomb repressive complexes restrain the expression of lineage-specific regulators in embryonic stem cells. Cell Cycle 5, 1411-1414.

Kim, J., Singh, A.K., Takata, Y., Lin, K., Shen, J., Lu, Y., Kerenyi, M.A., Orkin, S.H., Chen, T., 2015. LSD1 is essential for oocyte meiotic progression by regulating CDC25B expression in mice. Nat Commun 6, 10116.

Kohda, T., 2013. Effects of embryonic manipulation and epigenetics. J Hum Genet 58, 416-420.
Kojima, Y., Tam, O.H., Tam, P.P., 2014. Timing of developmental events in the early mouse embryo. Semin Cell Dev Biol 34, 65-75.
Lee, T.I., Jenner, R.G., Boyer, L.A., Guenther, M.G., Levine, S.S., Kumar, R.M., Chevalier, B., Johnstone, S.E., Cole, M.F., Isono, K., Koseki, H., Fuchikami, T., Abe, K., Murray, H.L., Zucker, J.P., Yuan, B., Bell, G.W., Herbolsheimer, E., Hannett, N.M., Sun, K., Odom, D.T., Otte, A.P., Volkert, T.L., Bartel, D.P., Melton, D.A., Gifford, D.K., Jaenisch, R., Young, R.A., 2006. Control of developmental regulators by Polycomb in human embryonic stem cells. Cell 125, 301-313.
Liu, J., An, L., Wang, J., Liu, Z., Dai, Y., Liu, Y., Yang, L., Du, F., 2019. Dynamic patterns of H3K4me3, H3K27me3, and Nanog during rabbit embryo development. Am J Transl Res 11, 430-441.
Liu, X., Wang, C., Liu, W., Li, J., Li, C., Kou, X., Chen, J., Zhao, Y., Gao, H., Wang, H., Zhang, Y., Gao, Y., Gao, S., 2016. Distinct features of H3K4me3 and H3K27me3 chromatin domains in pre-implantation embryos. Nature 537, 558-562.
Margueron, R., Li, G., Sarma, K., Blais, A., Zavadil, J., Woodcock, C.L., Dynlacht, B.D., Reinberg, D., 2008. Ezh1 and Ezh2 maintain repressive chromatin through different mechanisms. Mol Cell 32, 503-518.
Margueron, R., Reinberg, D., 2011. The Polycomb complex PRC2 and its mark in life. Nature 469, 343-349.
Matoba, S., Wang, H., Jiang, L., Lu, F., Iwabuchi, K.A., Wu, X., Inoue, K., Yang, L., Press, W., Lee, J.T., Ogura, A., Shen, L., Zhang, Y., 2018. Loss of H3K27me3 Imprinting in Somatic Cell Nuclear Transfer Embryos Disrupts Post-Implantation Development. Cell Stem Cell 23, 343-354.
Matsui, Y., Mochizuki, K., 2014. A current view of the epigenome in mouse primordial germ cells. Mol Reprod Dev 81, 160-170.
Mei, H., Kozuka, C., Hayashi, R., Kumon, M., Koseki, H., Inoue, A., 2021. H2AK119ub1 guides maternal inheritance and zygotic deposition of H3K27me3 in mouse embryos. Nat Genet 53, 539-550.
Meng, T.G., Zhou, Q., Ma, X.S., Liu, X.Y., Meng, Q.R., Huang, X.J., Liu, H.L., Lei, W.L., Zhao, Z.H., Ouyang, Y.C., Hou, Y., Schatten, H., Ou, X.H., Wang, Z.B., Gao, S.R., Sun, Q.Y., 2020. PRC2 and EHMT1 regulate H3K27me2 and H3K27me3 establishment across the zygote genome. Nat Commun 11, 6354.
Michalak, E.M., Burr, M.L., Bannister, A.J., Dawson, M.A., 2019. The roles of DNA, RNA and histone methylation in ageing and cancer. Nat Rev Mol Cell Biol 20, 573-589.
Mitsui, K., Tokuzawa, Y., Itoh, H., Segawa, K., Murakami, M., Takahashi, K., Maruyama, M., Maeda, M., Yamanaka, S., 2003. The homeoprotein Nanog is required for maintenance of pluripotency in mouse epiblast and ES cells. Cell 113, 631-642.
Mochizuki-Kashio, M., Aoyama, K., Sashida, G., Oshima, M., Tomioka, T., Muto, T., Wang, C., Iwama, A., 2015. Ezh2 loss in hematopoietic stem cells predisposes mice to develop heterogeneous malignancies in an Ezh1-dependent manner. Blood 126, 1172-1183.
Mole, M.A., Weberling, A., Zernicka-Goetz, M., 2020. Comparative analysis of human and mouse development: From zygote to pre-gastrulation. Curr Top Dev Biol 136, 113-138.
Morris, S.A., Grewal, S., Barrios, F., Patankar, S.N., Strauss, B., Buttery, L., Alexander, M., Shakesheff, K.M., Zernicka-Goetz, M., 2012. Dynamics of anterior-posterior axis formation in the developing mouse embryo. Nat Commun 3, 673.
O'Carroll, D., Erhardt, S., Pagani, M., Barton, S.C., Surani, M.A., Jenuwein, T., 2001. The polycomb-group gene Ezh2 is required for early mouse development. Molecular and cellular biology 21, 4330-4336.

Perez-Garcia, V., Fineberg, E., Wilson, R., Murray, A., Mazzeo, C.I., Tudor, C., Sienerth, A., White, J.K., Tuck, E., Ryder, E.J., Gleeson, D., Siragher, E., Wardle-Jones, H., Staudt, N., Wali, N., Collins, J., Geyer, S., Busch-Nentwich, E.M., Galli, A., Smith, J.C., Robertson, E., Adams, D.J., Weninger, W.J., Mohun, T., Hemberger, M., 2018. Placentation defects are highly prevalent in embryonic lethal mouse mutants. Nature 555, 463-468.

Picelli, S., Faridani, O.R., Bjorklund, A.K., Winberg, G., Sagasser, S., Sandberg, R., 2014. Full-length RNA-seq from single cells using Smart-seq2. Nat Protoc 9, 171-181.

Prokopuk, L., Stringer, J.M., White, C.R., Vossen, R., White, S.J., Cohen, A.S.A., Gibson, W.T., Western, P.S., 2018. Loss of maternal EED results in postnatal overgrowth. Clin Epigenetics 10, 95.

Rizzino, A., Wuebben, E.L., 2016. Sox2/Oct4: A delicately balanced partnership in pluripotent stem cells and embryogenesis. Biochim Biophys Acta 1859, 780-791.

Rossant, J., Cross, J.C., 2001. Placental development: lessons from mouse mutants. Nature reviews. Genetics 2, 538-548.

Rugg-Gunn, P.J., Cox, B.J., Ralston, A., Rossant, J., 2010. Distinct histone modifications in stem cell lines and tissue lineages from the early mouse embryo. Proc Natl Acad Sci U S A 107, 10783-10790.

Saitou, M., Kagiwada, S., Kurimoto, K., 2012. Epigenetic reprogramming in mouse pre-implantation development and primordial germ cells. Development 139, 15-31.

Santos, F., Peters, A.H., Otte, A.P., Reik, W., Dean, W., 2005. Dynamic chromatin modifications characterise the first cell cycle in mouse embryos. Dev Biol 280, 225-236.

Schuettengruber, B., Cavalli, G., 2009. Recruitment of polycomb group complexes and their role in the dynamic regulation of cell fate choice. Development 136, 3531-3542.

Shen, X., Liu, Y., Hsu, Y.J., Fujiwara, Y., Kim, J., Mao, X., Yuan, G.C., Orkin, S.H., 2008. EZH1 mediates methylation on histone H3 lysine 27 and complements EZH2 in maintaining stem cell identity and executing pluripotency. Mol Cell 32, 491-502.

Shibasaki, Y., Etoh, N., Hayasaka, M., Takahashi, M.O., Kakitani, M., Yamashita, T., Tomizuka, K., Hanaoka, K., 2009. Targeted deletion of the tybe IIb Na(+)-dependent Pi-co-transporter, NaPi-IIb, results in early embryonic lethality. Biochem Biophys Res Commun 381, 482-486.

Shin, J., Bossenz, M., Chung, Y., Ma, H., Byron, M., Taniguchi-Ishigaki, N., Zhu, X., Jiao, B., Hall, L.L., Green, M.R., Jones, S.N., Hermans-Borgmeyer, I., Lawrence, J.B., Bach, I., 2010. Maternal Rnf12/RLIM is required for imprinted X-chromosome inactivation in mice. Nature 467, 977-981.

Simon, J.A., Kingston, R.E., 2009. Mechanisms of polycomb gene silencing: knowns and unknowns. Nat Rev Mol Cell Biol 10, 697-708.

Tam, P.P., 1988. Postimplantation development of mitomycin C-treated mouse blastocysts. Teratology 37, 205-212.

Tam, P.P., Loebel, D.A., 2007. Gene function in mouse embryogenesis: get set for gastrulation. Nature reviews. Genetics 8, 368-381.

Tanaka, S., Kunath T Fau - Hadjantonakis, A.K., Hadjantonakis Ak Fau - Nagy, A., Nagy A Fau - Rossant, J., Rossant, J., 1998. Promotion of trophoblast stem cell proliferation by FGF4. Science 282, 2072-2075.

Tanaka, S., Oda, M., Toyoshima, Y., Wakayama, T., Tanaka, M., Yoshida, N., Hattori, N., Ohgane, J., Yanagimachi, R., Shiota, K., 2001. Placentomegaly in cloned mouse concepti caused by expansion of the spongiotrophoblast layer. Biol Reprod 65, 1813-1821.

Walentin, K., Hinze, C., Schmidt-Ott, K.M., 2016. The basal chorionic trophoblast cell layer: An emerging coordinator of placenta development. Bioessays 38, 254-265.

Wang, L.Y., Li, Z.K., Wang, L.B., Liu, C., Sun, X.H., Feng, G.H., Wang, J.Q., Li, Y.F., Qiao, L.Y., Nie, H., Jiang, L.Y., Sun, H., Xie, Y.L., Ma, S.N., Wan, H.F., Lu, F.L., Li, W., Zhou, Q., 2020. Overcoming Intrinsic H3K27me3 Imprinting Barriers Improves Post-implantation Development after Somatic Cell Nuclear Transfer. Cell Stem Cell 27, 315-325.

Xie, Z., Zhang, W., Zhang, Y., 2022. Loss of Slc38a4 imprinting is a major cause of mouse placenta hyperplasia in somatic cell nuclear transferred embryos at late gestation. Cell Rep 38, 110407.

Yan, J., Dutta, B., Hee, Y.T., Chng, W.J., 2019. Towards understanding of PRC2 binding to RNA. RNA Biol 16, 176-184.

Yu, J.R., Lee, C.H., Oksuz, O., Stafford, J.M., Reinberg, D., 2019. PRC2 is high maintenance. Genes Dev 33, 903-935.

Zenk, F., Loeser, E., Schiavo, R., Kilpert, F., Bogdanović, O., Iovino, N., 2017. Germ line-inherited H3K27me3 restricts enhancer function during maternal-to-zygotic transition. Science 357, 212-216.

Zhang, B., Zheng, H., Huang, B., Li, W., Xiang, Y., Peng, X., Ming, J., Wu, X., Zhang, Y., Xu, Q., Liu, W., Kou, X., Zhao, Y., He, W., Li, C., Chen, B., Li, Y., Wang, Q., Ma, J., Yin, Q., Kee, K., Meng, A., Gao, S., Xu, F., Na, J., Xie, W., 2016. Allelic reprogramming of the histone modification H3K4me3 in early mammalian development. Nature 537, 553-557.

Zheng, H., Huang, B., Zhang, B., Xiang, Y., Du, Z., Xu, Q., Li, Y., Wang, Q., Ma, J., Peng, X., Xu, F., Xie, W., 2016. Resetting Epigenetic Memory by Reprogramming of Histone Modifications in Mammals. Mol Cell 63, 1066-1079.

Zhu, M., Zernicka-Goetz, M., 2020. Principles of Self-Organization of the Mammalian Embryo. Cell 183, 1467-1478.

Figures

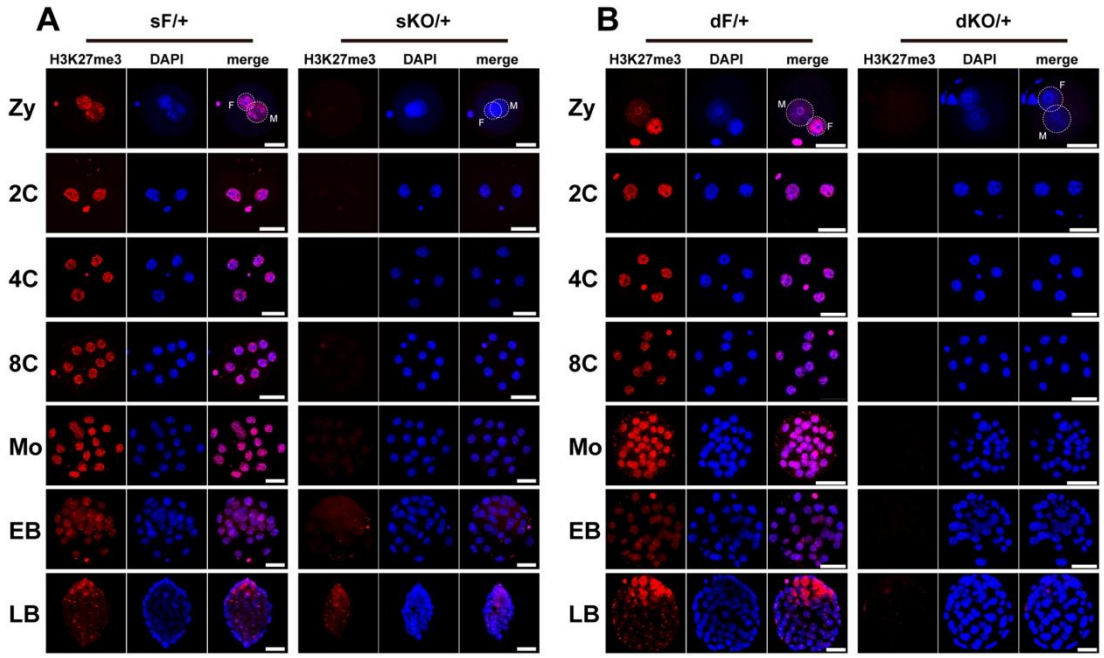

Figure 1. Delayed recovery of H3K27me3 modification in preimplantation stage of sKO/+ and dKO/+ embryos. (A) H3K27me3 patterns in sF/+ and sKO/+ embryos. In late zygotes, H3K27me3 was absent in both the male and female pronucleus (PN) of sKO/+. H3K27me3 was not detectable until late blastocysts in sKO/+ embryos. The number of zygotes examined: sF/+, n=22; sKO/+, n=21. 2-cell embryo: sF/+, n=21; sKO/+, n=25. 4-cell embryo: sF/+, n=26; sKO/+, n=12. 8-cell embryo: sF/+, n=12; sKO/+, n=16. Morula: sF/+, n=9; sKO/+, n=12. Early blastocyst: sF/+, n=9; sKO/+, n=18. Late blastocyst: sF/+, n=9; sKO/+, n=13. Scale bars, 50 μm. **(B)** H3K27me3 patterns in dF/+ and dKO/+ embryos. H3K27me3 was not detectable even in dKO/+ late blastocysts. Number of zygotes examined: dF/+, n=19; dKO/+, n=14. 2-cell embryo: dF/+, n=25; dKO/+, n=18. 4-cell embryo: dF/+, n=20; dKO/+, n=17. 8-cell embryo: dF/+, n=19; dKO/+, n=14. Morula: dF/+, n=31; dKO/+, n=38. Early blastocyst: dF/+, n=13; dKO/+, n=11. Late blastocyst: dF/+, n=4; dKO/+, n=11. Scale bars, 50 μm. Zy: zygote (PN4-PN5); 2C: 2-cell embryo; 4C: 4-cell embryo; 8C: 8-cell embryo; Mo: morula; EB: early blastocyst; LB: late blastocyst; M: male pronucleus; F: female pronucleus.

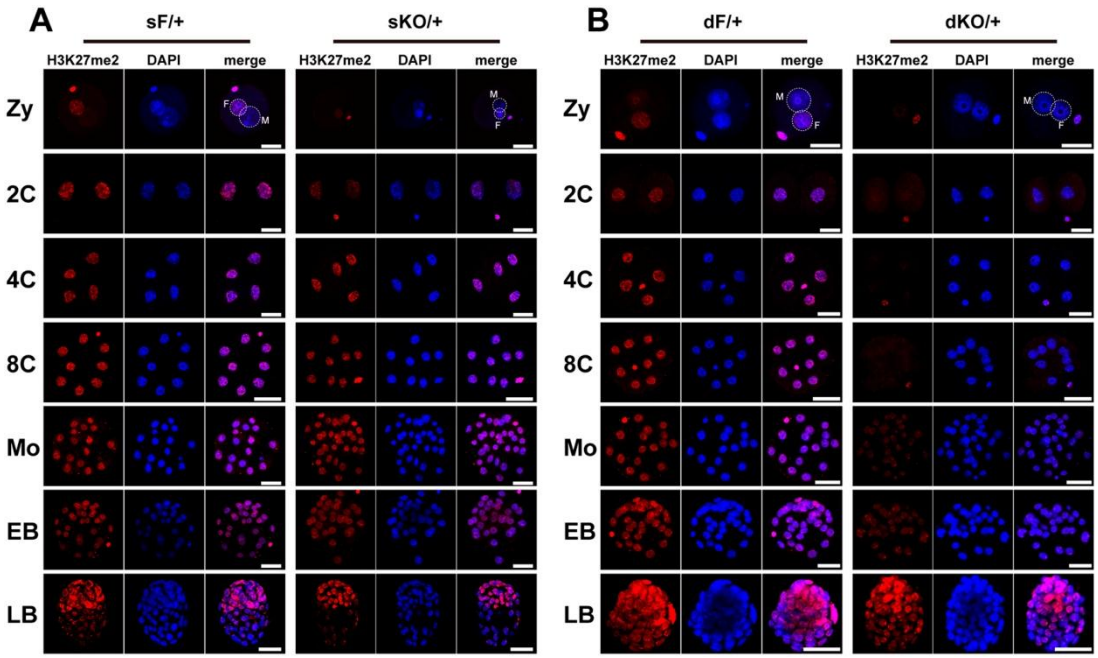

Figure 2. Delayed recovery of H3K27me2 modification in the preimplantation stage of sKO/+ and dKO/+ embryos. (A) H3K27me2 patterns in sF/+ and sKO/+ embryos. In sKO/+ late zygotes, H3K27me2 was undetectable in the male PN and faint in the female PN. H3K27me2 was recovered completely in 4-cell embryos in sKO/+. Number of zygotes examined: sF/+, n=21; sKO/+, n=20. 2-cell embryo: sF/+, n=38; sKO/+, n=19. 4-cell embryo: sF/+, n=30; sKO/+, n=13. 8-cell embryo: sF/+, n=36; sKO/+, n=44. Morula: sF/+, n=8; sKO/+, n=10. Early blastocyst: sF/+, n=12; sKO/+, n=5. Late blastocyst: sF/+, n=13; sKO/+, n=5. Scale bars, 50 μm. **(B)** H3K27me2 patterns in dF/+ and dKO/+ embryos. H3K27me2 in dKO/+ embryos was not detectable until the morula stage. Note dot signals in morulae and blastocysts. Number of zygotes examined: dF/+, n=17; dKO/+, n=10. 2-cell embryos: dF/+, n=12; dKO/+, n=13. 4-cell embryo: dF/+, n=20; dKO/+, n=8. 8-cell embryos: dF/+, n=11; dKO/+, n=14. Morula: dF/+, n=12; dKO/+, n=18. Early blastocysts: dF/+, n=12; dKO/+, n=5. Late blastocyst: dF/+, n=4; dKO/+, n=14. Scale bars, 50 μm. Zy: zygote (PN4-PN5); 2C: 2-cell embryo; 4C: 4-cell embryo; 8C: 8-cell embryo; Mo: morula; EB: early blastocyst; LB: late blastocyst; M: male pronucleus; F: female pronucleus.

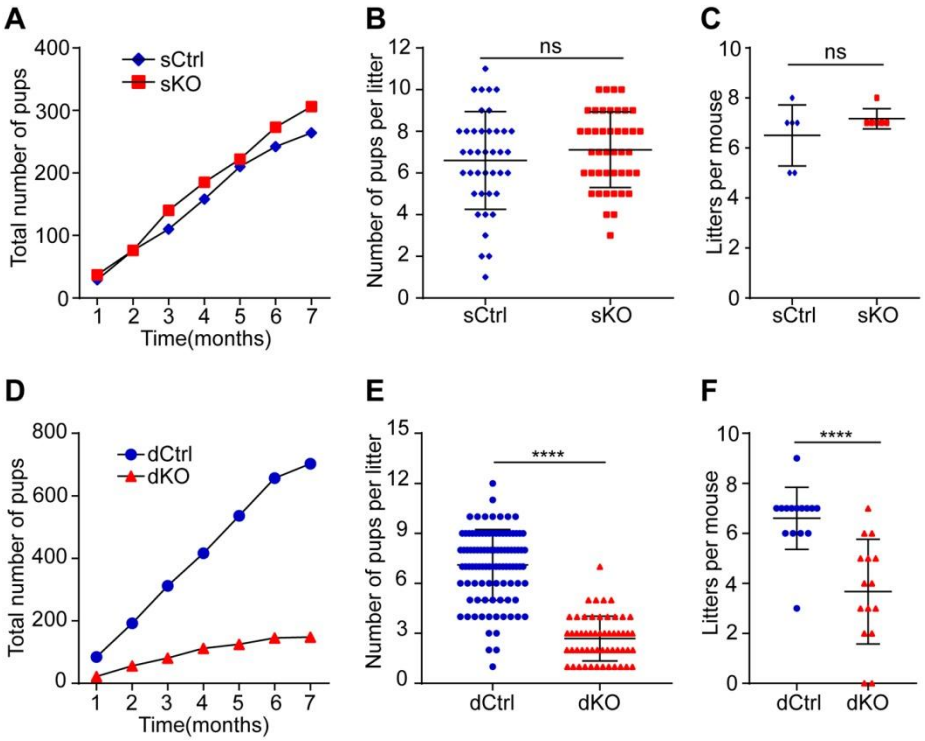

Figure 3. Double knockout of *Ezh1* and *Ezh2* in oocytes leads to female subfertility. (A-C) Fertility studies of sCtrl and sKO mice. Number of females: sCtrl, n=6; sKO, n=6. **(A)** The cumulative number of pups. **(B)** The average number of pups per litter. Data are presented as the mean ± SD. Mann-Whitney test: ns, not significant. **(C)** The average number of litters per mouse. Data are presented as the mean ± SD. Mann-Whitney test: ns, not significant. **(D-F)** Fertility studies of dCtrl and dKO mice. Number of females: dCtrl, n=15; dKO, n=15. **(D)** The cumulative number of pups. **(E)** The average number of pups per litter. Data are presented as the mean ± SD. Mann Whitney test: ****$P < 0.0001$. **(F)** The average number of litters per mouse. Data are presented as the mean ± SD. Mann-Whitney test: ****$P < 0.0001$.

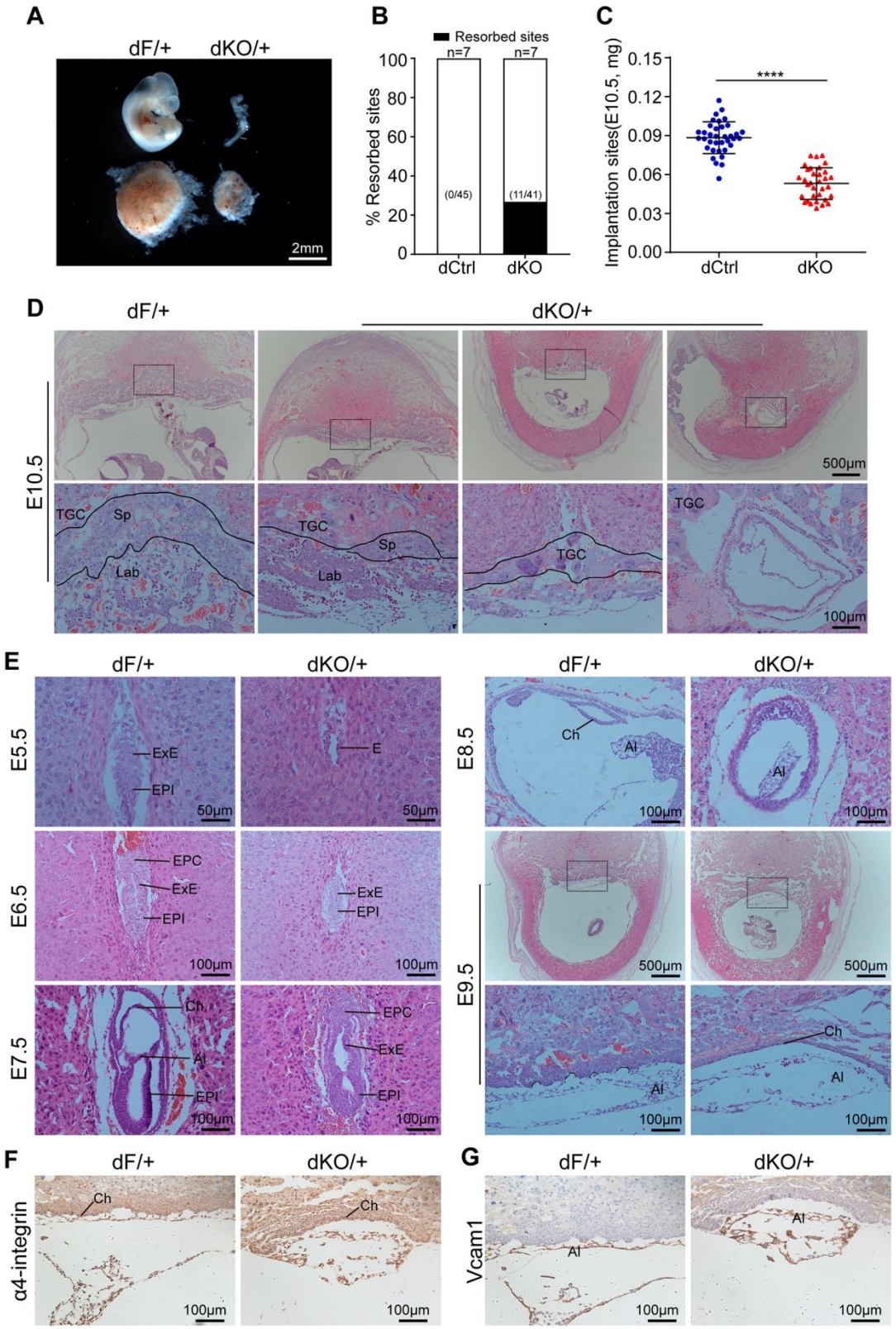

Figure 4. Double knockout of *Ezh1* and *Ezh2* in oocytes causes growth retardation during the postimplantation phase.

(A) Representative images of E10.5 fetuses (top) and placentae (bottom). **(B)** Ratio of

resorption sites at E10.5 in dCtrl and dKO females. Numbers within parentheses indicate the number of resorption sites over the total number of implantation sites. The number of females examined is shown on top of the bars. **(C)** The weight of implantation sites at E10.5. Number of implantation sites: dCtrl, n=36; dKO, n=33. The results are presented as the mean ± SD. Unpaired *t* test: ****$P < 0.0001$. **(D)** Representative images of placentae at E10.5 by HE staining. Black rectangles indicate the regions shown at higher magnification in the below panels. **(E)** Representative images of uterine decidua sections from E5.5 to E9.5 stained with HE. Black rectangles indicated the regions shown at higher magnification in the below panels. Lines at E9.5 in the bottom left indicate progression of labyrinth branching. The image in the bottom right shows failed branching. **(F)** The expression of Integrin α4 in the chorion at E9.5 by IHC staining. **(G)** Vcam1 expression in allantois at E9.5 by IHC staining. TGC, trophoblast giant cells; Sp, spongiotrophoblast; Lab, labyrinth; ExE, extraembryonic ectoderm; EPI, epiblast; E, embryo; EPC, ectoplacental cone; Ch, chorion; Al, allantois.

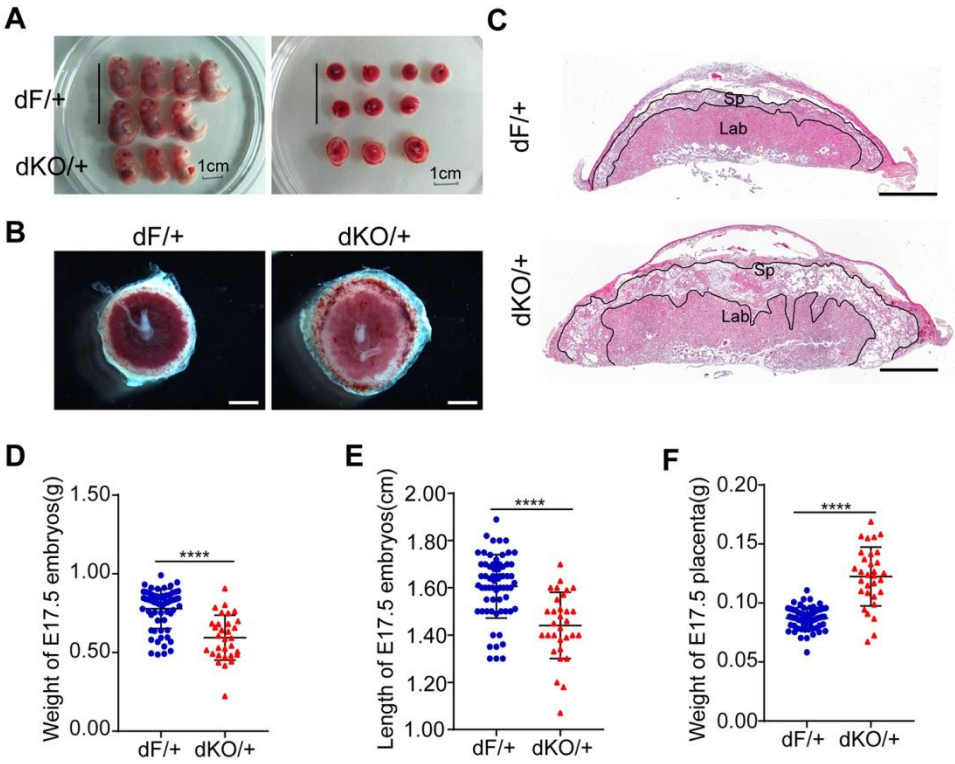

Figure 5. Placental enlargement in late stage of dKO/+ embryos. (A) Representative images of E17.5 fetuses and placentae. The top seven showed the dF/+ embryos, and the bottom three showed the dKO/+ embryos. **(B)** Representative images of E17.5 pacentae under the stereoscope. Scale bars, 1 mm. **(C)** Morphology of E17.5 placentae as evaluated by HE staining. Sp, spongiotrophoblast; Lab, labyrinth. Scale bars, 1 mm. **(D)** The weight of fetus at E17.5. The results are presented as the mean ± SD. Mann-Whitney test: ****$P < 0.0001$. **(E)** The length of fetus at E17.5. The results are presented as the mean ± SD. Mann-Whitney test: ****$P < 0.0001$. **(F)** The weight of placenta at E17.5. The results are presented as the mean ± SD. Unpaired *t* test: ****$P < 0.0001$.

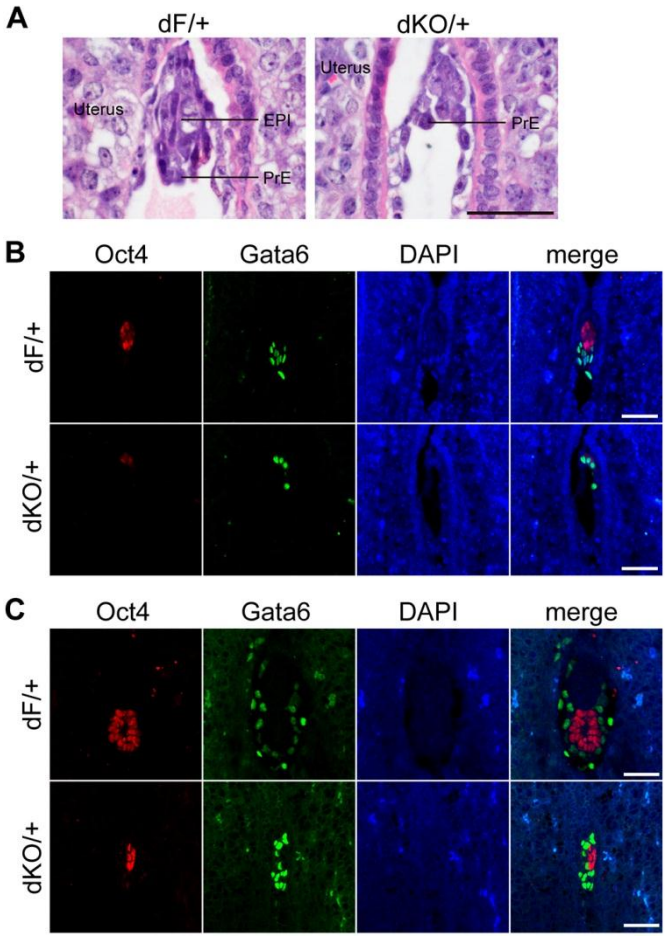

Figure 6. Development defects of epiblasts in postimplantation dKO/+ embryos. **(A)** HE staining of uterine decidua sections at E4.75. Scale bars, 50 μm. EPI: epiblast; PrE: primitive endoderm. **(B)** The expression of Oct4 and Gata6 in embryos at E4.75 by IF staining. Scale bars, 50 μm. **(C)** The expression of Oct4 and Gata6 in embryos at E5.5 by IF staining. Scale bars, 50 μm. Epiblast (EPI) cells were marked by Oct4 (red). Primitive endoderm (PrE) cells, visceral endoderm (VE) cells and parietal endoderm (PE) cells were marked by Gata6 (green).

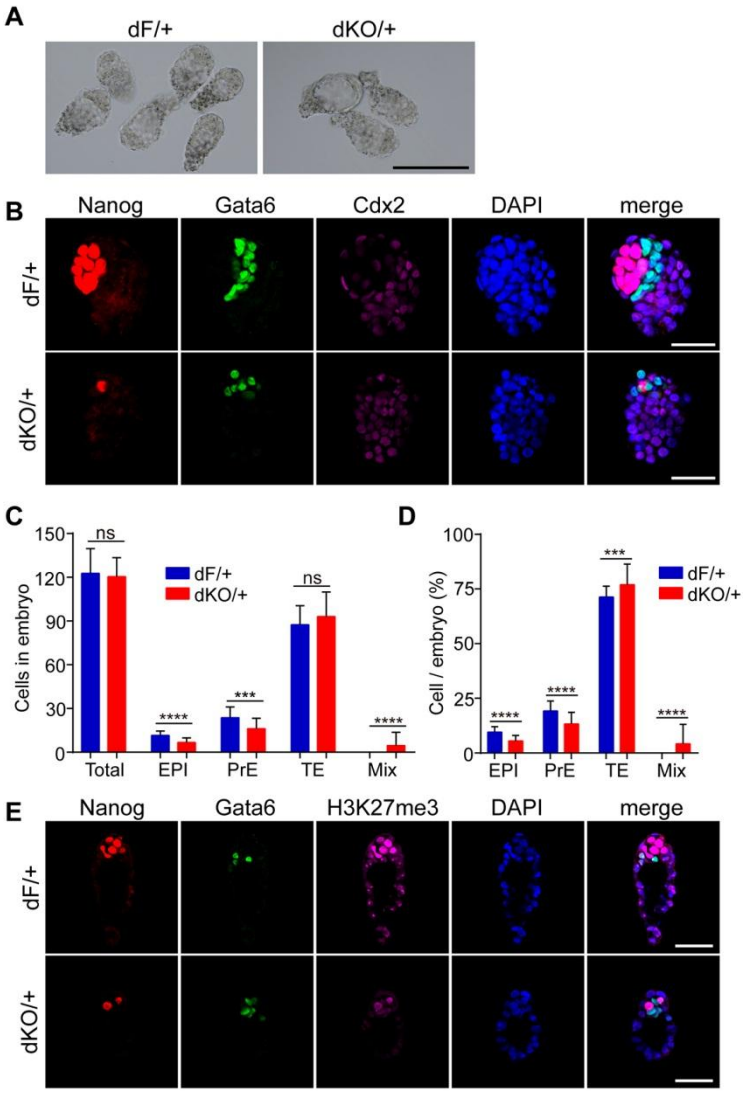

Figure 7. Decreased numbers of epiblast cells in dKO/+ embryos at E4.5. (A) Representative images of flushed embryos at E4.5. Scale bars, 50 μm. **(B)** Representative images of stem cell distribution in late blastocysts at E4.5. EPI cells were stained with Nanog (red), PrE cells were stained with Gata6 (green) and TE cells were stained with Cdx2 (magenta). Total number of embryos: dF/+, n=31; dKO/+, n=35. Scale bars, 50 μm. **(C)** The number of different cell parts in embryos. The results are presented as the mean ± SD. Statistical comparisons of values were made using Mann-Whitney test (Total, EPI, PrE and Mix) or unpaired *t* test (TE). ns, not significant. ***$P < 0.001$; ****$P < 0.0001$. **(D)** The ratio of different cell parts. The results are presented as the mean ± SD. Statistical comparisons of values were made using Mann-Whitney test (PrE, TE and Mix) or unpaired *t* test (EPI). ns, not

significant; ***P < 0.001; ****P < 0.0001. **(E)** Single optical sections of late blastocysts immunostained with Nanog, Gata6 and H3K27me3. Number of total embryos: dF/+, n=11; dKO/+, n=7.

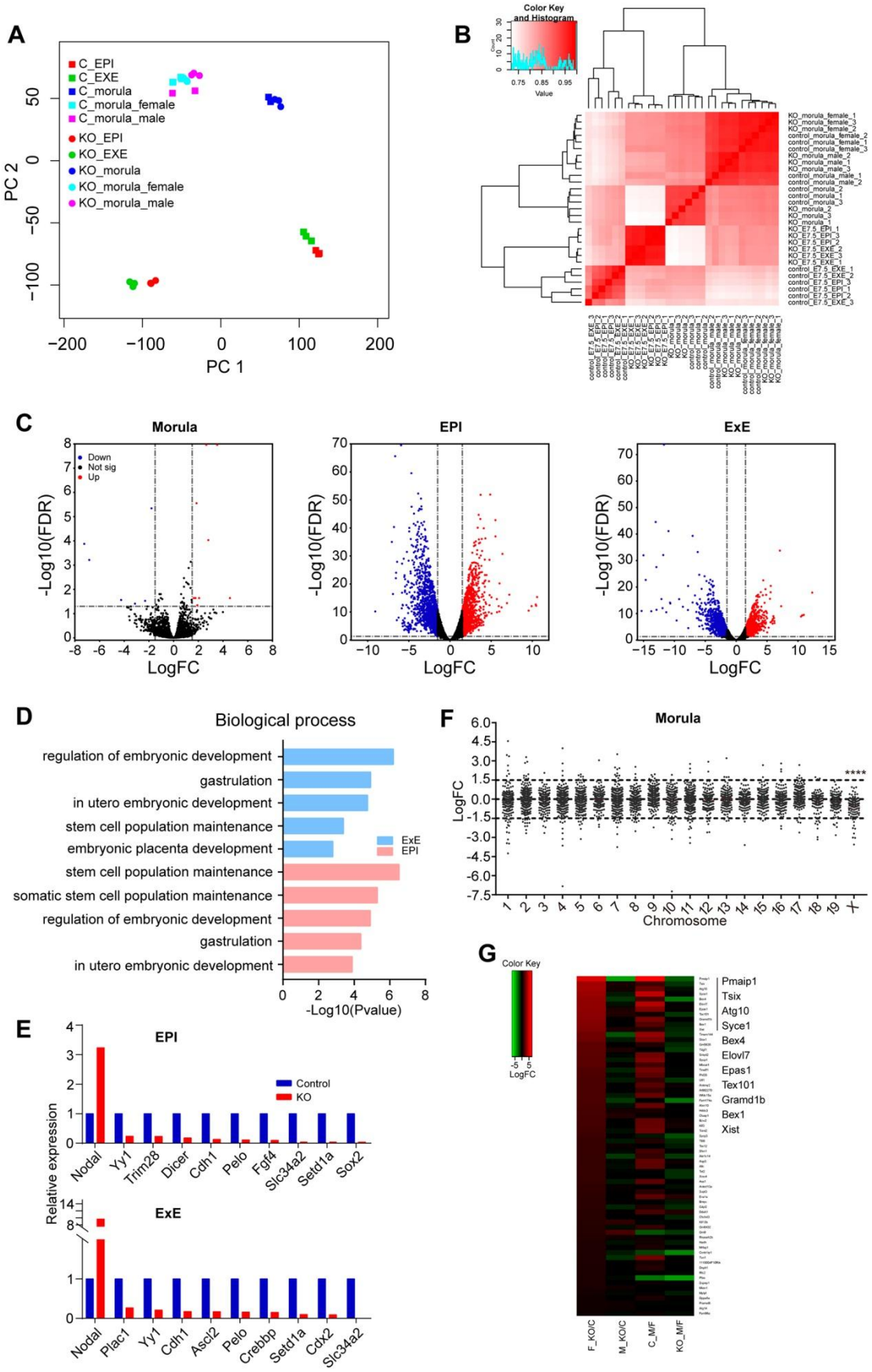

Figure 8. Transcriptomes and putative imprinted genes in dKO/+ embryos. (A) Principal component analysis (PCA) comparison between all samples. **(B)** Correlation between biological replicates of RNA-seq samples. **(C)** Volcano plot comparing RNA transcripts in control and KO embryos. Cutoff: FDR < 0.05 and | logFC | > 1.5. This is plotted by http://www.bioinformatica.com.cn. **(D)** Biological process associated with stem cells and development at E7.5. GO was analyzed in Metascape. **(E)** Relative expression levels of genes associated with stem cells and development by RNA-seq at E7.5. The expression level of the control was set as 1. **(F)** Relative gene expression levels of morula from chromosomes 1 to X (excluding Y). One-way ANOVA test: ****P < 0.0001. **(G)** Heatmap showing putative H3K27me3-dependent imprinted genes at the morula stage. Control_morula, Control_E7.5_EPI and Control_E7.5_ExE are from dF/+ embryos. KO_morula, KO_E7.5_EPI and KO_E7.5_ExE are from dKO/+ embryos. Control_morula_male and Control_morula_female are from pronucleus exchange of dF/+ zygotes. KO_morula_male and KO_morula_female are from pronucleus exchange of dKO/+ zygotes. C, control; F, female; M, male.

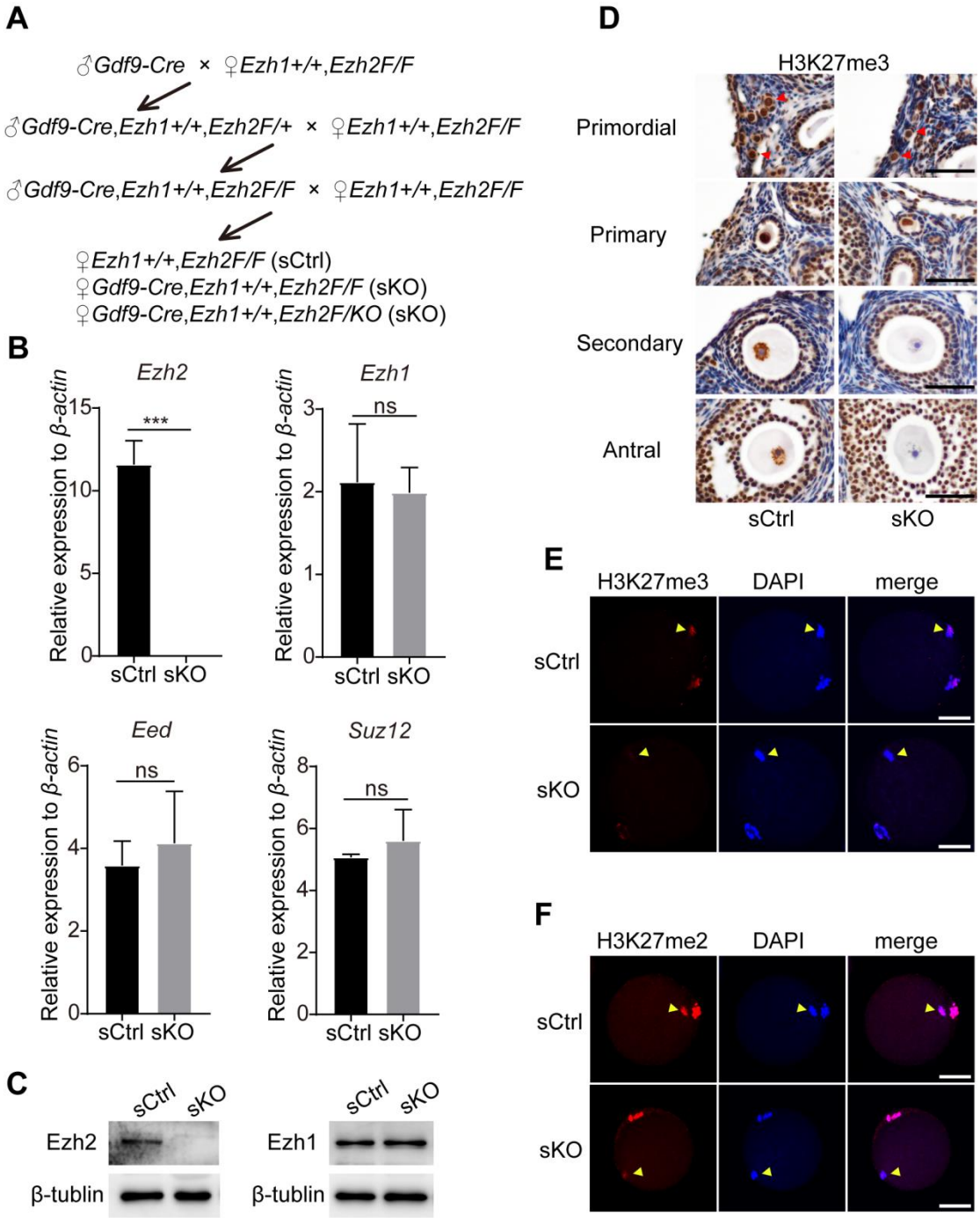

Fig. S1. Generation of maternal *Ezh2* deficient mice and knockout efficiency in oocytes. (A) Breeding scheme used to generate sCtrl and sKO mice. **(B)** Real-time PCR analysis of mRNA level for *Ezh2*, *Ezh1*, *Eed* and *Suz12* in sCtrl and sKO oocytes. Data are presented as the mean ± SD. Unpaired *t* test: ns, not significant; ***$P < 0.001$. **(C)** Levels of Ezh2 and Ezh1 protein in oocytes as assessed by western blot analysis; β-tublin was used as loading control. **(D)** H3K27me3 in

oocytes from primordial, primary, secondary and antral follicles checked by immunohistochemical (IHC) staining. Ovary sections were stained with anti-H3K27me3 antibody and counterstained with hematoxylin. The primordial follicles were indicated by red arrows. Scale bars, 50 μm. **(E and F)** H3K27me3 and H3K27me2 in super-ovulated oocytes measured by immunofluorescence (IF) staining. The chromosomes of oocytes were indicated by yellow arrows. Number of oocytes examined for H3K27me3: sCtrl, n=27; sKO, n=21. For H3K27me2: sCtrl, n=16; sKO, n=20. Scale bars, 50 μm.

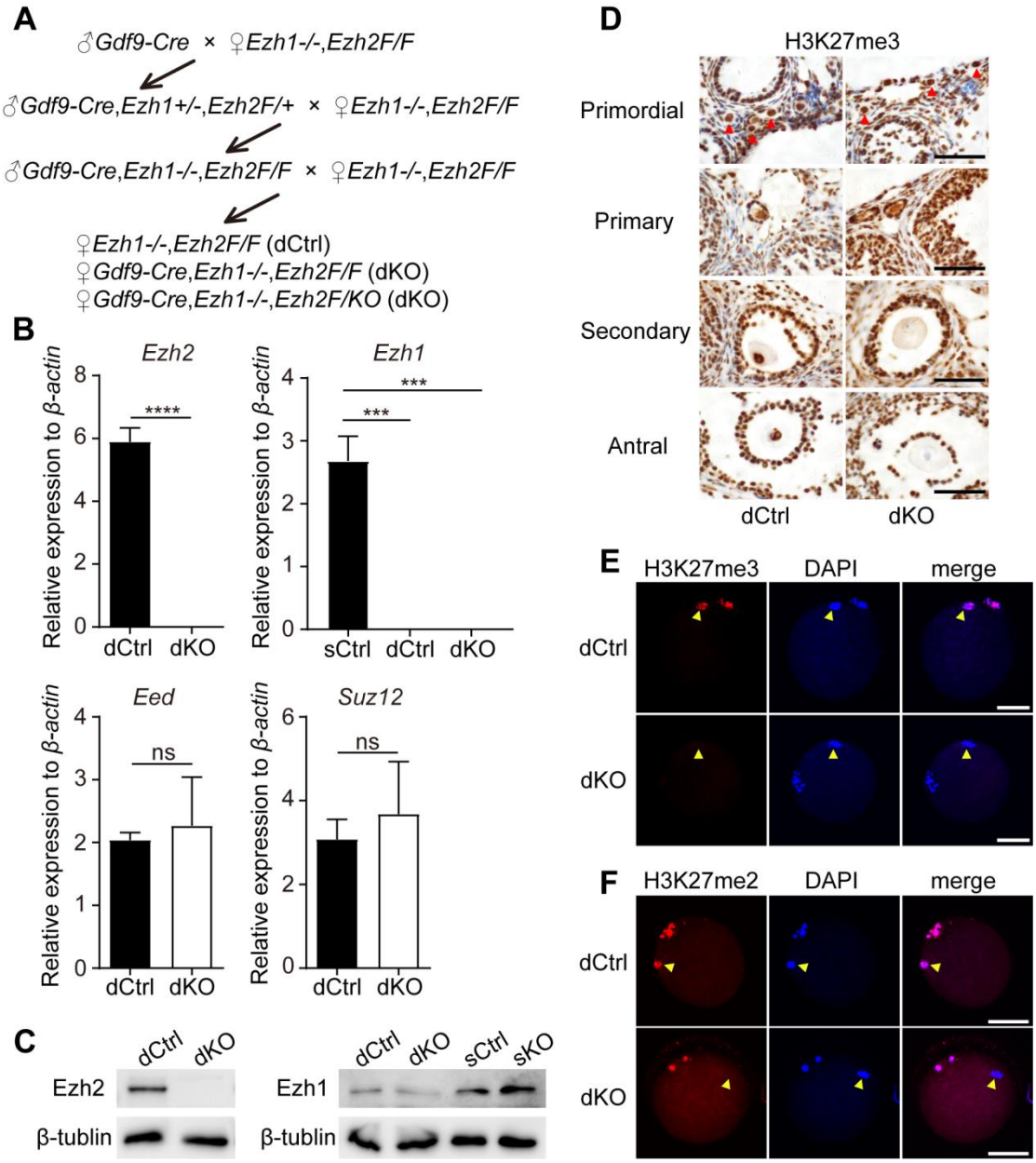

Fig. S2. Generation of maternal *Ezh1/2* deficient mice and knock out efficiency in oocytes. (A) Breeding scheme used to generate dCtrl and dKO mice. **(B)** Real-time PCR analysis of *Ezh2*, *Ezh1*, *Eed* and *Suz12* transcripts in dCtrl and dKO oocytes. Data are presented as the mean ± SD. Unpaired *t* test: ns, not significant; ***$P < 0.001$; ****$P < 0.0001$. **(C)** Levels of Ezh2 and Ezh1 protein in oocytes as assessed by western blot analysis; β-tublin was used as loading control. **(D)** IHC staining showed H3K27me3 modification in oocytes from primordial, primary, secondary and antral follicles. Ovary sections were stained with anti-H3K27me3 antibody and then counterstained with hematoxylin. The primordial follicles were indicated by red arrows. Scale bars, 50 μm. **(E and F)** IF analysis of H3K27me3 and H3K27me2 in super-ovulated oocytes. The chromosomes of oocytes were indicated by yellow arrows. Number of oocytes examined for H3K27me3: dCtrl, n=16; dKO, n=28. For H3K27me2: dCtrl, n=24; dKO, n=32. Scale bars, 50μm.

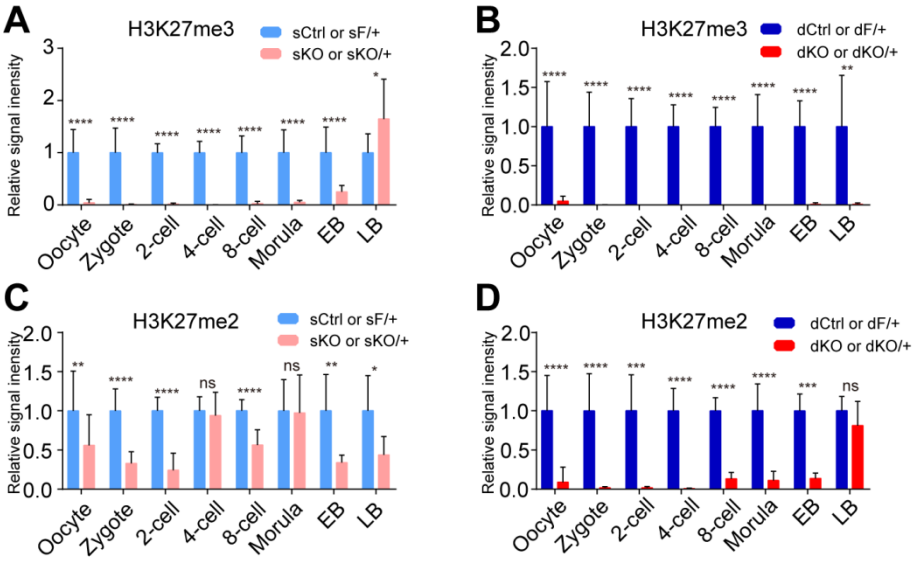

Fig. S3. The relative level of H3K27me3 and H3K27me2 signals in oocytes and embryos. (A) Relative H3K27me3 signal intensity in single knockout groups. (B) Relative H3K27me3 signal intensity in double knockout groups. (C) Relative H3K27me2 signal intensity in single knockout groups. (D) Relative H3K27me2 signal intensity in double knockout groups. EB, early blastocyst; LB, late blastocyst. The average siganls of control oocytes or embryos were set as 1.0. Results are presented as mean ± SD. Mann Whitney test or unpaired *t* test: ns, not significant; **P* < 0.05; ***P* < 0.01; ****P* < 0.001; *****P* < 0.0001.

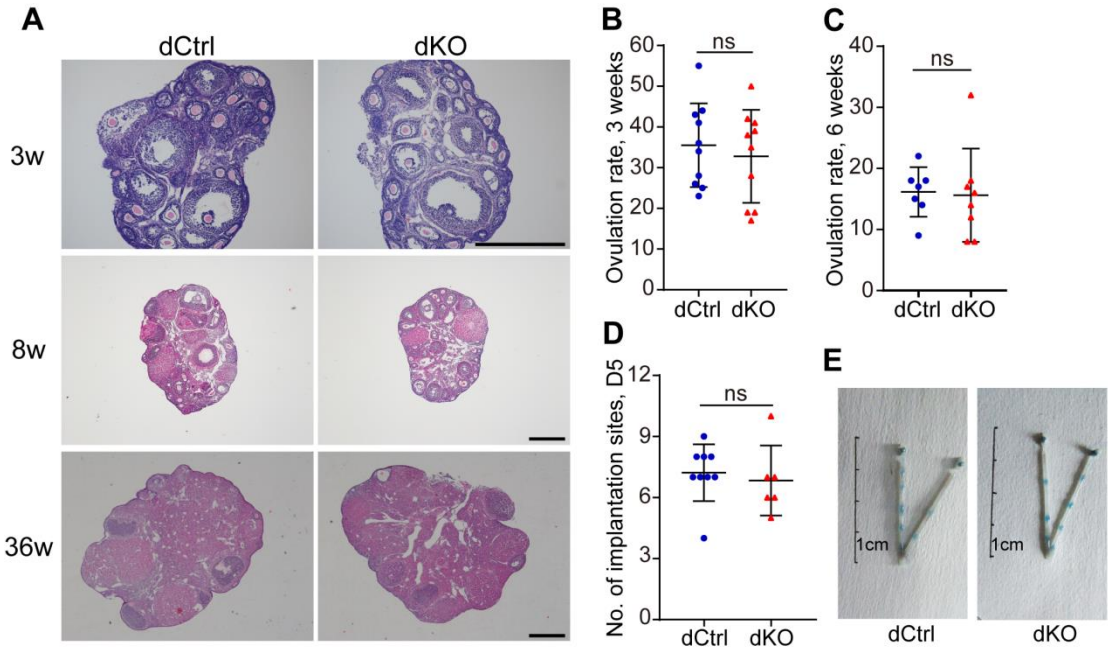

Fig. S4. Ovary morphology, ovulation rate and implantation site in dCtrl and dKO female mice. (A) Ovary sections stained with hematoxylin-rosin (HE) from 3-, 8-, and 36-wk-old mice. 3-wk-old mice were treated with PMSG for 46 hours. Scale bars, 500 μm. **(B and C)** The number of ovulated oocytes per female mouse with superovulation treatment. **(D)** The number of implantation sites on Day 5 of pregnancy in dCtrl and dKO mice. **(E)** Representative images of uteri with implantation sites on Day 5. Scale bars, 1cm. Results are presented as mean ± SD. Statistical comparisons of values were made using unpaired *t* test (B and C) or Mann Whitney test (D). ns, not significant.

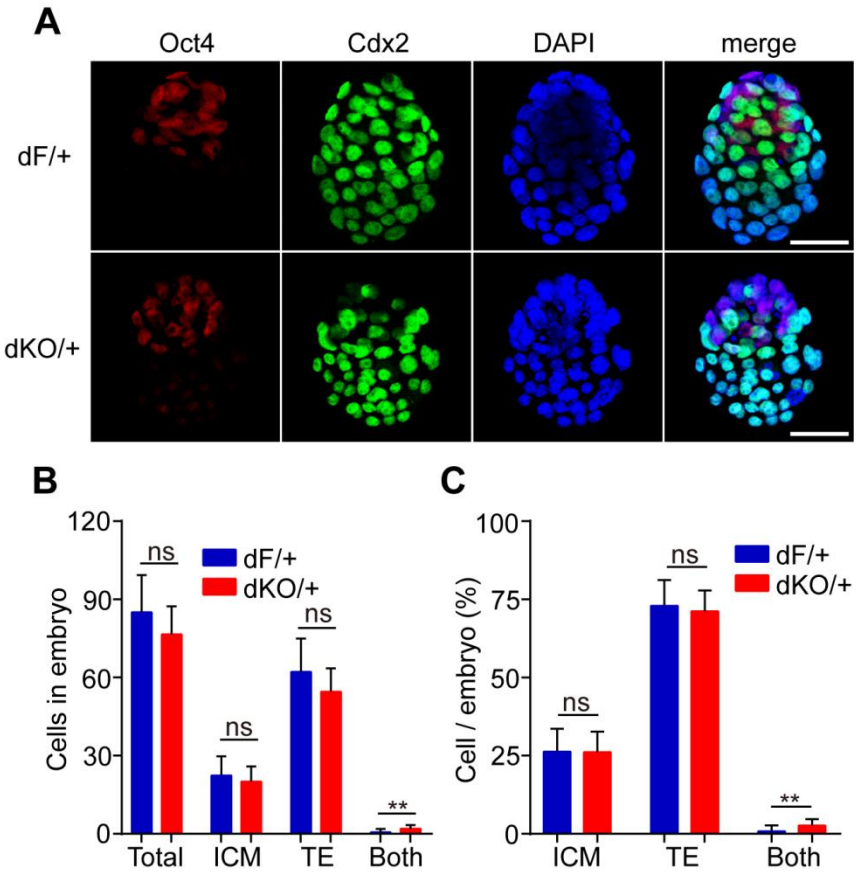

Fig. S5. The normal differentiation of trophectoderm (TE) and the inner cell mass (ICM) in dKO/+ embryos at E3.75. (A) Representative images of Oct4 and Cdx2 immunostaining in embryos at E3.75. Inner cell mass (ICM) were stained with Oct4 (red) and trophectoderm (TE) cells were stained with Cdx2 (green). Number of total embryos: dF/+, n=13; dKO/+, n=11. Scale bars, 50 μm. **(B)** The number of different cell parts in embryos at E3.75. Results are presented as mean ± SD. Statistical comparisons of values were made using Mann Whitney test (Total and Both) or unpaired *t* test (ICM and TE). ns, not significant; $^{**}P < 0.01$. **(C)** The proportion of different cell parts at E3.75. Both: mix-expression of Oct4 and Cdx2. Results are presented as mean ± SD. Statistical comparisons of values were made using Mann Whitney test (Both) or unpaired *t* test (ICM and TE). ns, not significant; $^{**}P < 0.01$.

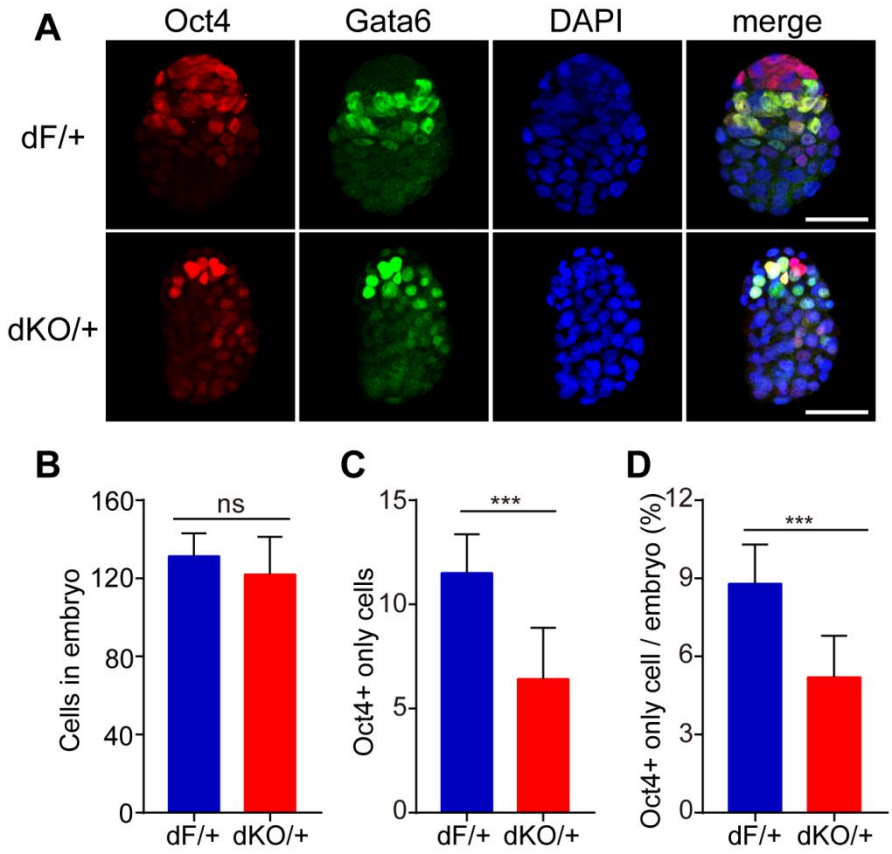

Fig. S6. Oct4+ only cells were decreased at E4.5. (A) Representative images of Oct4 and Gata6 in embryos at E4.5. ICM cells were labled by Oct4 (red) and PrE cells were marked by Gata6 (green). Number of total embryos: dF/+, n=6; dKO/+, n=19. Scale bars, 50 μm. **(B)** The average number of total cells in embryos. Results are presented as mean ± SD. Mann Whitney test: ns, not significant. **(C)** Decreased Oct4+ only cells in dKO/+ embryos. Results are presented as mean ± SD. Mann Whitney test: ***$P < 0.001$. (D) Ratio of EPI cells classified by Oct4+ only cells. Results are presented as mean ± SD. Mann Whitney test: ***$P < 0.001$.

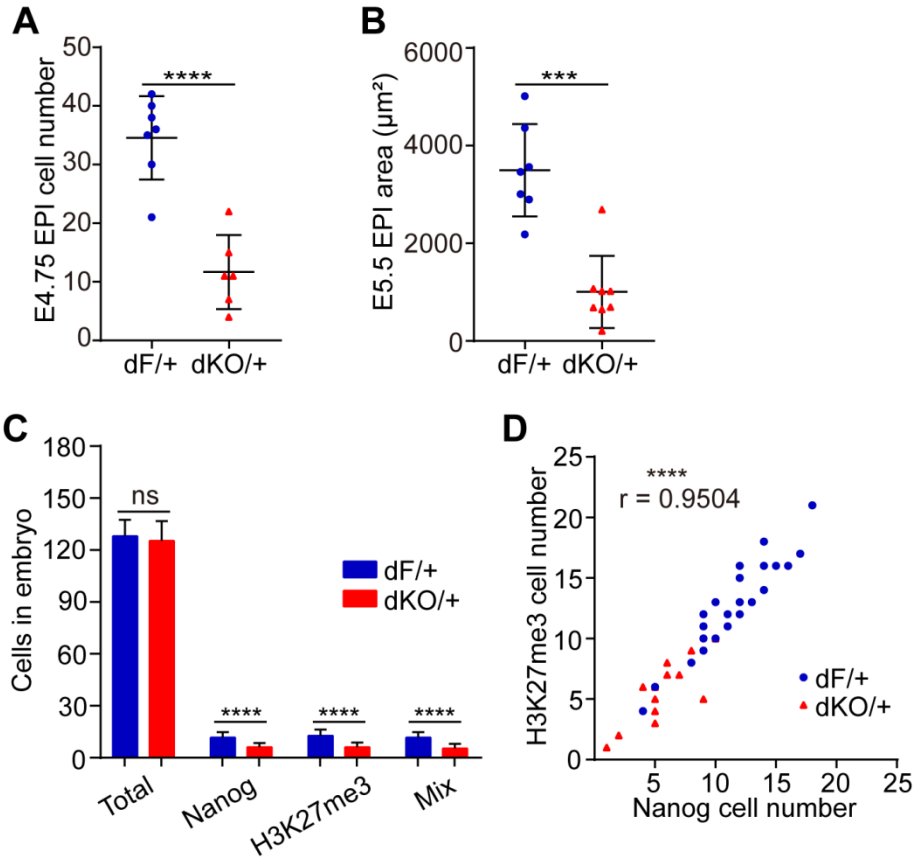

Fig. S7. Decreased EPI cells from E4.5 to E5.5. (A) EPI cell number at E4.75. Number of total embryos: dF/+, n=7; dKO/+, n=6. Results are presented as mean ± SD. Unpaired *t* test: ****$P < 0.0001$. **(B)** EPI area at E5.5. Results are presented as mean ± SD. Mann Whitney test: ***$P < 0.001$. **(C)** Decreased Nanog and H3K27me3 cells in dKO/+ embryos. Mix: cells showed both Nanog and H3K27me3 staining. Results are presented as mean ± SD. Unpaired *t* test: ns, not significant; ****$P <$ 0.0001. **(D)** Correlation analysis of Nanog and H3K27me3 cell numbers. Number of total embryos: dF/+, n=31; dKO/+, n=17. The cell numbers is highly correlated; Pearson r = 0.9504. ****$P < 0.0001$.

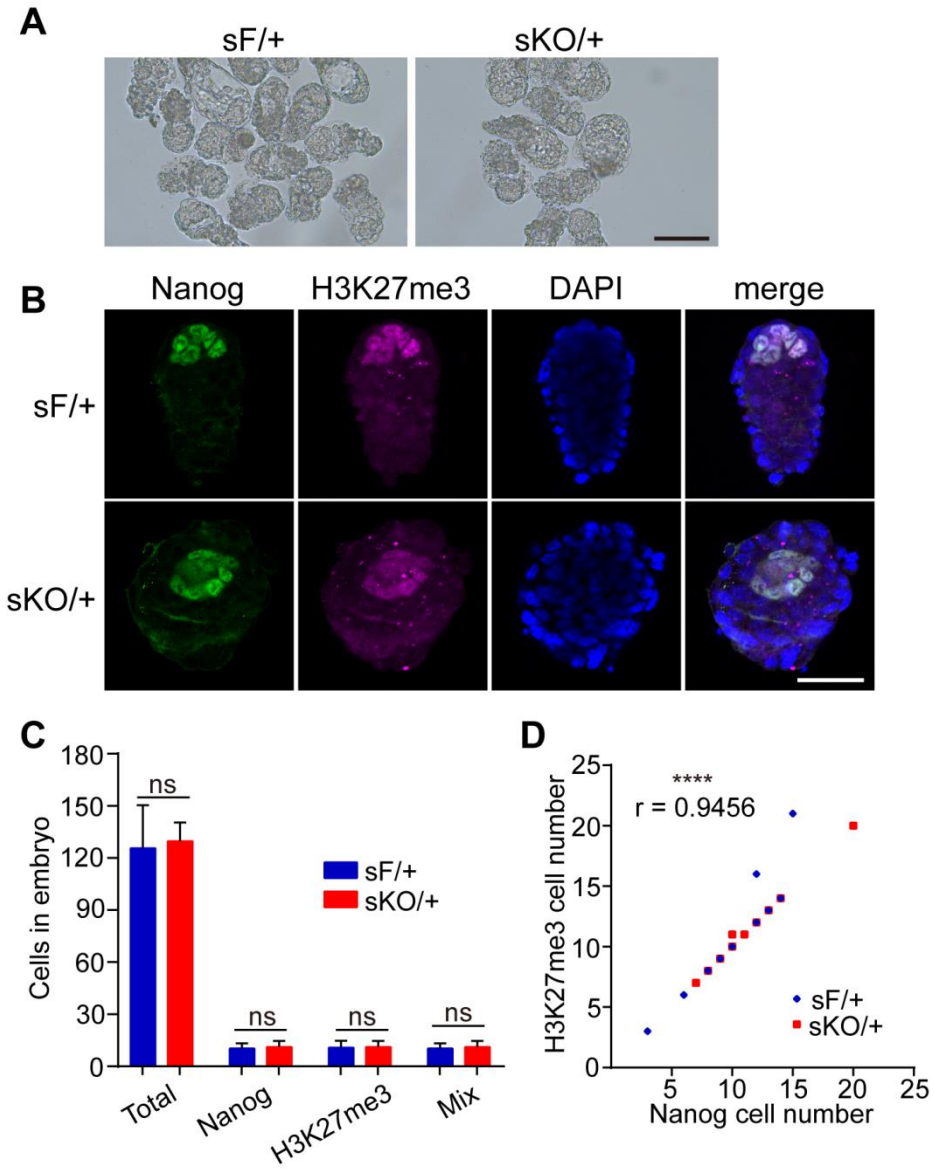

Fig. S8. Normal epiblast cells in sKO/+ Embryos at E4.5. (A) Representative images of flushed embryos at E4.5. Scale bars, 100 μm. **(B)** Representative images of late blastocysts immunostained with Nanog and H3K27me3. Number of total embryos: sF/+, n=31; sKO/+, n=35. Scale bars, 50 μm. **(C)** Quantitative analysis of Nanog and H3K27me3 cells. Mix: cells showed both Nanog and H3K27me3 staining. Results are presented as mean ± SD. Mann Whitney test: ns, not significant. **(D)** Correlation analysis of Nanog and H3K27me3 cell numbers. Number of total embryos: sF/+, n=31; sKO/+, n=35. The cell numbers is highly correlated; Pearson r = 0.9456. ****$P < 0.0001$.

Table S1. Embryo transfer

Group	No. of recipients	No. of blastocysts transferred	Pups per littter	Term pups (%)
dF/+	13	170	6.31±2.32	82 (48.24%)
dKO/+	9	111	2.22±1.86***	20 (18.02%)****

Pups per recipient are recorded as mean ± SD. Statistical comparisons were made using Mann Whitney test, ***$P < 0.001$. Comparisons between dF/+ and dKO/+ about Pups (%) were by χ^2 test, ****$P < 0.0001$.

Table S2. Primers

Gene	Sequence (5′ to 3′)	Reference
Primers for genotype		
Ezh2-F	GCTAGAAGCATTCCCCACAC	
Ezh2-R	CTGGCTCTGTGGAACCAAAC	
Ezh2-R (within *lacZ*)	ATGGGCCTCATAGTGACAGG	
Ezh1-F	GATGCCCTCAACCAGTACTC	
Ezh1-R	TTTATATCACGCACCCACAC	
Ezh1-R (within *lacZ*)	TAAAGCGAGTGGCAACATGG	
Gdf9-Cre-F	TCTGATGAAGTCAGGAAGAACC	
Gdf9-Cre-R	GAGATGTCCTTCACTCTGATTC	
Internal control-F	CAAATGTTGCTTGTCTGGTG	
Internal control-R	GTCAGTCGAGTGCACAGTTT	
Primers for real-time PCR		
Ezh2-F	TGACCCTGACCTCTGTCTCACG	
Ezh2-R	TCAGACGGTGCCAGCAGTAAGT	
Ezh1-F	AGCGATGCTGTGTTTCTGGA	
Ezh1-R	GGCGCTTCCGTTTTCTTGTT	
Eed-F	ATGCCATTGTATGCTGGAAACC	
Eed-R	CACTGGCTGTAATCAAATCGCC	
Suz12-F	TCTCATCGAAATTCCAGAACAAGC	
Suz12-R	CAAGCTATGAGATTCTTGCTCTCC	
β-actin-F	GTGACGAGGCCCAGAGCAAGAG	(1)
β-actin-R	CGTACATGGCTGGGGTGTTGAAGG	

Table S3. Antibodies

Antibody	Source	Concentration
Rabbit polyclonal Anti-Ezh2	Abcam, ab186006	WB: 1:500
Mouse monoclonal Anti-beta tublin	Proteintech, 66240	WB: 1:2000
Rabbit monoclonal Anti-H3K27me3	CST, 9733	IHC: 1:2500
		IF: 1:400
Rabbit monoclonal Anti-Vcam1	Abcam, ab134047	IHC: 1:1000
Rabbit polyclonal Anti-integrin alpha 4	Santa Cruz, sc14008	IHC: 1:1000
Rabbit monoclonal Anti-H3K27me2	CST, 9728	IF: 1:400
Rabbit monoclonal Anti-Oct4	Abcam, ab200834	IF: 1:200
Mouse monoclonal Anti-Cdx2	Biogenex, CDX-88	IF: 1:200
Rabbit polyclonal Anti-Nanog	Abcam, ab80892	IF: 1:200
Goat polyclonal Anti-Gata6	R&D systems, AF1700	IF: 1:200
Alexa Fluor 594 Goat Anti-Rabbit IgG	ZSBIO, ZF-0516	IF: 1:200
Alexa Fluor 488 Goat Anti-Mouse IgG	ZSBIO, ZF-0516	IF: 1:200
Alexa Fluor 568 Donkey Anti-Rabbit IgG (H+L)	Abcam, ab175693	IF: 1:500
Alexa Fluor 594 Donkey Anti-Rabbit IgG (H+L)	YEASEN, 34212ES60	IF: 1:200
Alexa Fluor 488 Donkey Anti-Goat IgG (H+L)	YEASEN, 34306ES60	IF: 1:200
Alexa Fluor 647 Donkey Anti-Mouse IgG (H+L)	YEASEN, 34113ES60	IF: 1:200

Table S4.

Click here to download Table S4

Reference

1. Ciccone DN, Su H, Hevi S, Gay F, Lei H, Bajko J, et al. KDM1B is a histone H3K4 demethylase required to establish maternal genomic imprints. Nature. 2009;461(7262):415-8.